# Stochastic quantum trajectories demonstrate the quantum Zeno effect in open spin 1/2, spin 1 and spin 3/2 systems

OPEN ACCESS
IOP Publishing
Journal of Physics A: Mathematical and Theoretical
J. Phys. A: Math. Theor. **57** (2024) 175301 (30pp)
https://doi.org/10.1088/1751-8121/ad3ab4

# Stochastic quantum trajectories demonstrate the quantum Zeno effect in open spin 1/2, spin 1 and spin 3/2 systems

**Sophia M Walls*, Julien M Schachter, Haocheng Qian and Ian J Ford**

Department of Physics and Astronomy, University College London, Gower Street, London WC1E 6BT, United Kingdom

E-mail: sophia.walls.17@ucl.ac.uk

Received 31 January 2023; revised 29 March 2024
Accepted for publication 4 April 2024
Published 18 April 2024

**Abstract**

We investigate the quantum Zeno effect (QZE) in spin 1/2, spin 1 and spin 3/2 open quantum systems undergoing Rabi oscillations, revealing unexplored features for the spin 1 and spin 3/2 systems. The systems interact with an environment designed to perform continuous measurements of an observable, driving the systems stochastically towards one of the eigenstates of the corresponding operator. The system-environment coupling constant represents the strength of the measurement. Stochastic quantum trajectories are generated by unravelling a Markovian Lindblad master equation using the quantum state diffusion formalism. These are regarded as a more appropriate representation of system behaviour than consideration of the averaged evolution since the latter can mask the effect of measurement. Complete positivity is maintained and thus the trajectories can be considered as physically meaningful. The QZE is investigated over a range of measurement strengths. Increasing the strength leads to greater system dwell in the vicinity of the eigenstates of the measured observable and lengthens the time taken by the system to return to that eigenstate, thus the QZE emerges. For very strong measurement, the Rabi oscillations resemble randomly occurring near-instantaneous jumps between eigenstates. The trajectories followed by the quantum system are heavily dependent on the measurement strength which other than slowing down and adding noise to the Rabi oscillations, changes the paths taken in spin phase space from a circular

* Author to whom any correspondence should be addressed.

precession into elaborate figures-of-eight. For spin 1 and spin 3/2 systems, the measurement strength determines which eigenstates are explored and the QZE is stronger when the system dwells in the vicinity of certain eigenstates compared to others.

Keywords: the quantum Zeno effect, stochastic quantum trajectories, quantum state diffusion, open quantum systems

## 1. Introduction

The quantum Zeno effect (QZE), also known as the Turing Paradox, is the suppression of the unitary time evolution of a system brought about by repeated measurements. The first general derivation of the QZE was performed by Degasperis *et al* in 1974 [1] but the effect was formally characterised by Misra and Sudarshan [2], who showed in 1977 that the probability that a system should remain in an initial state will approach unity as the frequency of projective measurements made on it tends to infinity. The QZE was named after the Greek philosopher Zeno's paradox, which suggested that if an arrow were continuously observed, it would (arguably) appear to be motionless and thus would never reach its target. Any disturbance in the rate of change of a quantum system as a result of measurement can be considered to be a demonstration of the QZE or the quantum anti-Zeno effect, the latter corresponding to the opposite of the QZE and manifesting itself as the speeding up of the system dynamics rather than the slowing down. It has also been demonstrated that the QZE may be exhibited through a series of frequent, partial, incomplete measurements, such that an incomplete wavefunction collapse leads the system to be more likely to remain in its initial state [3, 4].

A notable motivation for understanding the QZE is that it might be used to stabilise quantum systems in a particular state such that properties of the system such as entanglement and coherence might be maintained [5, 6]. The stability of such properties is of great importance in quantum error correction algorithms or quantum teleportation, as well as in many other quantum computational fields [7–10]. A recent use of the QZE was demonstrated by Blumenthal *et al* [11]. It was shown that the joint evolution of at least two non-interacting qubits could be achieved through the continuous measurement of one qubit, such that the operation becomes a multi-qubit entangling gate. A similar effect was found by Nodurft *et al* whereby polarisation entanglement could be generated between two initially unentangled photons in coupled waveguides through the QZE [12]. Finally, the QZE has been frequently studied in electron spins in quantum dots, trapped ions and nuclear spins, and Markovian and non-Markovian open quantum system dynamics [13–16].

The conceptual difficulty with studying the QZE theoretically is that the conventional quantum mechanical framework consists of two distinct regimes. The unitary time evolution of the quantum system governed by the internal Hamiltonian is described by the deterministic, time-reversal symmetric Schrödinger equation, whilst measurement of the quantum system is introduced as an interruption of the unitary evolution of the quantum system in a discontinuous, indeterministic and irreversible manner via the Born rule [17]. With the consequences of measurement of the system being absent from the dynamical equation of motion and average quantities masking the effect of measurement, it is not straightforward to characterise how the unitary evolution is influenced by measurement [17, 18].

To reveal the effects of measurement on a system's unitary evolution, an approach that enables the study of single, physically realistic quantum trajectories is required. Many experimental and theoretical works have investigated quantum trajectories [19–23]. Presilla *et al* compared the experimental results of the QZE found by Itano *et al* on a two-level system

with the theoretical predictions formulated through the path-integral and QSD formalisms [24, 25]. It was found that that the experimental results of Itano *et al* correspond to a high measurement coupling strength between the system and the measuring apparatus. Snizhko *et al.* recently illustrated, through the study of quantum trajectories, that the QZE includes a number of transition stages leading to an increase in qubit survival probability [26]. Gambetta *et al* also studied the QZE of a superconducting charged qubit coupled to a transmission line resonator with a Rabi control drive, undergoing weak homodyne measurements, which illustrated the competition between the measurement drive and the Rabi oscillation system dynamics [27].

Approaches exist where individual trajectories are employed to generate the evolution of the (reduced) density matrix of a system averaged over environmental conditions, but often these are not regarded as physically realistic: for example the Stochastic Liouville-von Neumann Equation is based on an evolving ensemble of density matrices that do not preserve unit trace and thus are not physically meaningful [28]. Quantum jump trajectories can also be generated which consist of intervals of piecewise deterministic evolution interrupted by stochastic, discontinuous jumps [29, 30]. More recently, a new method of generating trajectories, namely *jump-time unravellings,* has emerged whereby quantum trajectories are bundled together and averaged over at specific points in time where jumps occur [31]. In this work, we instead turn to quantum state diffusion (QSD), also known as weak measurement [32]. QSD offers continuous stochastic quantum trajectories and a dynamical treatment of measurement instead of instantaneous wavefunction collapse. For example, near instantaneous jumps have been observed in diffusive trajectories of a quantum system generated by QSD [33]. Bauer *et al* and Spiller have demonstrated that the QZE is a phenomenon that naturally arises in a spin 1/2 system treated within the QSD framework [34, 35]. We extend this by demonstrating the QZE, and its dependence on the strength of measurement coupling, in spin systems higher than spin 1/2 and reveal novel features that emerge only in the higher spin systems.

QSD considers quantum systems that are in contact with an environment that causes the system reduced density matrix to *diffuse* across its parameter space. Environmental effects in QSD can drive phenomena such as decoherence and the (continuous) collapse of the system to a particular eigenstate, all within a single dynamical framework. An average over all possible diffusive trajectories then yields the evolution of the density matrix of the quantum system as given by the Lindblad equation, at least for Markovian dynamics.

For our purposes, we consider the environment to represent a measuring apparatus, and the strength of the interaction between the quantum system and environment to be a measurement coupling that brings about the diffusion of the system towards a stochastically selected eigenstate. Rather than the system collapsing discontinuously to an eigenstate, as is the case with projective measurements, the measurement process occurs in a continuous and non-instantaneous manner. An approximation to instantaneous wavefunction collapse is obtained in the limit of infinitely strong system-environment coupling. Near-instantaneous quantum jumps are recovered in this limit (not to be confused with the intrinsically discontinuous Poissonian jump unravelling of a quantum master equation) [27, 29, 30]. The QSD evolution equation for the system therefore contains not only the unitary time evolution brought about, for example, by a system Hamiltonian, but also the effect of measurement.

The probabilistic nature of the measurement process is represented as stochastic noise in the QSD framework, generating dynamics described by stochastic differential equations (SDEs) or Itô processes when the stochasticity is Markovian [32]. The origin of such a stochasticity might be interpreted as pseudo-random rather than truly indeterministic since the noise that is introduced into the system dynamics could be a reflection of the underspecified state of the environment with which the system is interacting, rather like the noise experienced by an open system like a Brownian particle in classical mechanics. Within such a framework

we consider the stochastically evolving density matrix to be a physically real property of the quantum system [36–43], instead of merely a tool to calculate the average evolution or representing the (subjective) state of our knowledge [44–52], which is still the subject of debate, also in the context of quantum trajectories [17, 53–57]. Nevertheless, results obtained from QSD are consistent with the Born rule, and are therefore compatible with the axioms of quantum mechanics.

In this study of the QZE, we employ QSD to study spin 1/2, spin 1 and spin 3/2 systems, each undergoing Rabi oscillations while coupled to a measuring device that monitors the component of spin along the $z$-axis. We derive SDEs for the expectation values of the three Cartesian components of the spin operator, but reinterpret these quantities as stochastic properties of the system associated with individual quantum trajectories as opposed to averages over multiple realisations of the noise or equivalently over an ensemble of adoptable density matrices. The quantum trajectories of each of these systems are used to observe the effects of increased measurement coupling on the unitary dynamics of the system. In particular, the stochastic quantum trajectories are analysed to calculate the probabilities of system residence in the vicinity of $z$-spin eigenstates, the average time taken by the system to return to such an eigenstate, and how these quantities depend on the measurement strength.

The plan for the paper is as follows. Section 2 summarises the key ideas of QSD and SDEs, and section 3 provides a specification of the parametrisation and dynamics of the spin systems. Section 4 describes the quantum trajectories obtained using such a framework and through an analysis of such trajectories presents insights into the QZE. Our conclusions are given in section 5.

## 2. Quantum state diffusion and a stochastic Lindblad equation

### *2.1. Open quantum systems and the Kraus operator formalism*

Open quantum systems are ubiquitous since most systems can be found interacting with their environment. The complexity of this interaction as well as uncertainty in the initial state of the environment mean that an element of randomness enters into the description of the environment's influence on a quantum system. This motivates a description of the open quantum system using a randomly evolving (reduced) density matrix.

In order to develop these ideas, consider the commonly used evolution of the density matrix $\rho(t)$ defined through the action of the super-operator $S$ in a time interval d$t$. Such a mapping of states of the quantum system must preserve the unit trace and positivity for the quantum state to be considered physically meaningful [58]. The action of the super-operator on $\rho$ can be expressed as

$$S[\rho(t)] = \rho(t+dt) = \sum_j M_j(\mathrm{d}t)\,\rho(t)\,M_j^\dagger(\mathrm{d}t)\,. \tag{1}$$

The Kraus operators $M_j(\mathrm{d}t)$ represent all possible transitions brought about by the system dynamics together with system-environment interactions and can in principle be derived from terms in the Hamiltonian. In order to preserve the trace of $\rho$ they must satisfy the completeness relation $\sum_j M_j^\dagger M_j = \mathbb{I}$. The Kraus operators depend on $dt$ and, for continuous evolution of the density matrix, must differ by a small perturbation from the identity operator $\mathbb{I}$. For simplicity we use the set of Kraus operators $M_l \equiv M_{k\pm}(\mathrm{d}t) = \frac{1}{\sqrt{2}}(\mathbb{I} + A_{k\pm})$, where $k$ labels a particular Lindblad channel $k$, with the $\pm$ subscript representing two possible measurement outcomes or transitions associated with the interaction. We employ $A_{k\pm} = -iH_s\mathrm{d}t - \frac{1}{2}L_k^\dagger L_k \mathrm{d}t \pm L_k\sqrt{\mathrm{d}t}$

where $H_s$ is the system Hamiltonian and $L_k$ the operator associated with the $k$th Lindblad channel [18, 59–61]. The use of two Kraus operators per Lindblad channel is reminiscent of the approach used by Wiseman, namely Kraus operators $\Omega_{k1} = \sqrt{\mathrm{d}t}L_k$ and $\Omega_{k0} = \mathbb{I} - (iH_s + \frac{1}{2}L_k^\dagger L_k)\mathrm{d}t$ [56], such that $\Omega_{k1} = \frac{1}{\sqrt{2}}(M_{k+} - M_{k-})$ and $\Omega_{k0} = \frac{1}{\sqrt{2}}(M_{k+} + M_{k-})$. Note that the Kraus operators $\Omega_{k0,1}$ and $M_{k\pm}$ yield the same Lindblad master equation but differ in their stochastic realisations of the trajectories, where the former produces discontinuous, 'jump-like' trajectories and the latter diffusive, continuous trajectories.

Such a positive map then results in the ubiquitous Lindblad master equation describing the Markovian evolution of the reduced density matrix $\rho$ averaged over the measurement outcomes:

$$\mathrm{d}\rho = -i\,[H_s, \rho]\,\mathrm{d}t + \sum_k \left( L_k \rho L_k^\dagger - \frac{1}{2}\left\{ L_k^\dagger L_k, \rho \right\} \right) \mathrm{d}t. \tag{2}$$

The density operator $\rho$ may be regarded as representing a statistical ensemble of the pure states that could be adopted by an open quantum system after a measurement has been performed. As such, the Lindblad master equation describes the average evolution of this ensemble under the action of the Kraus operators.

Another possible interpretation of equation (1), when written as

$$\rho\,(t + dt) = \sum_l p_l\,(\mathrm{d}t)\,\frac{M_l\,(\mathrm{d}t)\,\rho\,(t)\,M_l^\dagger\,(\mathrm{d}t)}{Tr\left(M_l\,(\mathrm{d}t)\,\rho\,(t)\,M_l^\dagger\,(\mathrm{d}t)\right)}, \tag{3}$$

is that the dynamics may be represented as stochastic transitions from $\rho(t)$ to $M_l(\mathrm{d}t)\rho(t)M_l^\dagger(\mathrm{d}t)/Tr(M_l(\mathrm{d}t)\rho(t)M_l^\dagger(\mathrm{d}t))$ that occur with a probability $p_l(\mathrm{d}t) = Tr(M_l(\mathrm{d}t)\rho(t)M_l^\dagger(\mathrm{d}t))$ that depends on the density matrix of the system at time $t$. Equation (1) represents the average evolution of the density matrix as a result of the action of all the Kraus operators on $\rho(t)$. Stochastic quantum trajectories might then be generated through a series of transitions employing a sequence of Kraus operators. This is a strategy that has been used in studies of evolving quantum systems [56, 58].

Our strategy is to generate trajectories reflecting a single possible evolution path of $\rho$ rather than an averaged one, and so we take the stochastic interpretation just mentioned. We are modelling measurement as an interaction between a system and its environment that affects the system in a manner not dissimilar to the effect of a host medium on a Brownian particle. Such an approach can make sense since the state of the environment is unknown, giving rise to an evolving uncertainty in the state of the quantum system. To reflect such an uncertainty it would be natural to consider an ensemble of density matrices at each point in time $t$, reflecting the multiple possible states of the system as a result of lack of knowledge of the state of the environment. Similarly to Matos *et al* [59], the average of such an ensemble of density operators may be denoted by the over-bar, $\bar{\rho}$. The evolution of the ensemble averaged density matrix over a time increment $dt$ would then be expressed as [59]

$$\bar{\rho}\,(t + \mathrm{d}t) = \sum_l M_l\,(\mathrm{d}t)\,\bar{\rho}\,(t)\,M_l^\dagger\,(\mathrm{d}t)\,. \tag{4}$$

In contrast, the action of a single Kraus operator on a member $\rho(t)$ of such an ensemble represents one of a set of possible system evolutions:

$$\rho(t+\mathrm{d}t) = \rho(t) + \mathrm{d}\rho = \frac{M_l(\mathrm{d}t)\,\rho(t)\,M_l^\dagger(\mathrm{d}t)}{Tr\left(M_l(\mathrm{d}t)\,\rho(t)\,M_l^\dagger(\mathrm{d}t)\right)}, \tag{5}$$

and a sequence of such transformations can generate a single, possible evolution path of $\rho$. Note that the preservation of the trace and positivity of the standard Kraus operator map of equation (1) is well-known [58]. Trace preservation is apparent also in equation (5). However, preservation of positivity in the action of a single Kraus operator of the form $M_{k\pm}(dt) = \frac{1}{\sqrt{2}}(\mathbb{I} + A_{k\pm})$ on one member of an ensemble of density matrices in equation (5) remains to be demonstrated and will be shown in the following.

Consider a density matrix $\rho(t)$ at a time $t$, specified to be completely positive and hence to have only non-negative eigenvalues. The determinant of such a density matrix is $\det(\rho(t)) = \prod_i \lambda_i$ where $\lambda_i$ denote the eigenvalues of $\rho(t)$. The determinant of $\rho(t)$ is thus positive. Now we consider the determinant of the density matrix at time $t+\mathrm{d}t$, namely $\rho(t+\mathrm{d}t)$ generated according to equation (5) by a Kraus operator of the form stated above $M = C(\mathbb{I}+A)$, where $A$ is infinitesimal (in the sense that $A \to 0$ as $\mathrm{d}t \to 0$) and $C$ is a constant, such that $\tilde{M} = M/C = \mathbb{I} + A$ differs infinitesimally from the identity $\mathbb{I}$. We write

$$\rho(t+\mathrm{d}t) = \frac{\tilde{M}\rho(t)\tilde{M}^\dagger}{Tr\left(\tilde{M}\rho(t)\tilde{M}^\dagger\right)}, \tag{6}$$

and employ the identity $\det(\exp A) = \exp(TrA)$ such that $\det(\mathbb{I}+A) \approx 1 + Tr(A)$ for infinitesimal $A$, whereby

$$\begin{aligned}
\det(\rho(t+\mathrm{d}t)) &= \frac{\det\left(\tilde{M}\right)\det(\rho(t))\det\left(\tilde{M}^\dagger\right)}{Tr\left(\tilde{M}\rho(t)\tilde{M}^\dagger\right)} \\
&\approx \frac{(1+Tr(A))\det(\rho(t))\left(1+Tr\left(A^\dagger\right)\right)}{Tr\left(\tilde{M}^\dagger\tilde{M}\rho(t)\right)} \\
&\approx \frac{\left(1+Tr\left(A+A^\dagger\right)\right)\det(\rho(t))}{Tr\left((\mathbb{I}+A+A^\dagger)\rho(t)\right)} \\
&= \frac{\left(1+Tr(A+A^\dagger)\right)\det(\rho(t))}{1+Tr((A+A^\dagger)\rho(t))} \\
&\approx \det(\rho(t))\left[1+Tr(A+A^\dagger) - Tr((A+A^\dagger)\rho(t))\right].
\end{aligned} \tag{7}$$

Next we note that an unacceptable map would produce a density matrix with at least one negative eigenvalue. We can therefore identify unphysical dynamics if a density matrix is generated whose determinant passes through zero at some point in time. This includes cases where an odd number of eigenvalues change sign simultaneously (such that the determinant becomes negative) or where an even number do so (such that the determinant goes through a cusp at zero).

So let us examine the dynamics represented by equation (7). It can be demonstrated that the determinant of $\rho(t+\mathrm{d}t)$ can never go to zero within a finite time-frame, under certain conditions. We express the change in the determinant of the density matrix $d\det(\rho) = \det(\rho(t+\mathrm{d}t)) - \det(\rho(t))$ as an Itô process: $\mathrm{d}\det(\rho) = \det(\rho)(a\mathrm{d}t + b\mathrm{dW})$, where dW is a

Wiener increment and $a$ and $b$ are specified functions. Letting $y = \ln(\det(\rho))$, the following SDE for $y$ may be obtained:

$$\mathrm{d}y = \frac{1}{\det(\rho)}\mathrm{d}\det(\rho) + \frac{1}{2}b^2\det(\rho)^2\left(-\frac{1}{\det(\rho)^2}\right)\mathrm{d}t = a\mathrm{d}t + b\mathrm{dW} - \frac{1}{2}b^2\mathrm{d}t. \tag{8}$$

The unacceptable behaviour $\det(\rho) \to 0$ corresponds to $y \to -\infty$ and unless $a$ or $b$ possess singularities it is clear that this can only emerge, if at all, as $t \to \infty$. Thus the dynamics of the single Kraus operator map, equation (5), with $M = C(\mathbb{I} + A)$ and employing a non-singular, infinitesimal $A$, are physically acceptable.

Employing the set of Kraus operators from before, $M_{k\pm} = \frac{1}{\sqrt{2}}(\mathbb{I} + A_{k\pm})$ and $A_{k\pm} = -iH_s\mathrm{d}t - \frac{1}{2}L_k^\dagger L_k\mathrm{d}t \pm L_k\sqrt{\mathrm{d}t}$, [58–60] yields the following Lindblad equation:

$$\mathrm{d}\bar{\rho} = -i[H_s, \bar{\rho}]\,\mathrm{d}t + \sum_k \left(L_k\bar{\rho}L_k^\dagger - \frac{1}{2}\left\{L_k^\dagger L_k, \bar{\rho}\right\}\right)\mathrm{d}t, \tag{9}$$

which explicitly describes the evolution of an average over the ensemble of density matrices. We generate stochastic trajectories by *unravelling* equation (9) in the manner of equation (5) such that an equation concerning a single member of the ensemble of density matrices $\rho(t)$ can be formulated. We next derive such an equation for $\rho(t)$ in the form of an Itô process.

### 2.2. Unravelled stochastic Lindblad equation

We unravel the deterministic Lindblad equation by implementing the stochastic evolution of $\rho$ according to the set of available transitions

$$\rho(t + dt) = \frac{M_{k\pm}(\mathrm{d}t)\,\rho(t)\,M_{k\pm}^\dagger(\mathrm{d}t)}{Tr\left(M_{k\pm}(\mathrm{d}t)\,\rho(t)\,M_{k\pm}^\dagger(\mathrm{d}t)\right)}, \tag{10}$$

each adopted with probability $p_{k\pm}(\mathrm{d}t) = Tr(M_{k\pm}(\mathrm{d}t)\rho(t)M_{k\pm}^\dagger(\mathrm{d}t))$. The outcome is an Itô process for $\rho$ involving independent Wiener increments $\mathrm{dW_k}$ (in the case of more than one Lindblad operator) [59]:

$$\begin{aligned}\mathrm{d}\rho = -i[H_s, \rho]\,\mathrm{d}t + \sum_k \Bigg(&\left(L_k\rho L_k^\dagger - \frac{1}{2}\left\{L_k^\dagger L_k, \rho\right\}\right)\mathrm{d}t \\ &+ \left(\rho L_k^\dagger + L_k\rho - Tr\left[\rho\left(L_k + L_k^\dagger\right)\right]\rho\right)\mathrm{dW}_k\Bigg).\end{aligned} \tag{11}$$

Solutions to this equation describe possible stochastic quantum trajectories of the reduced system density matrix $\rho$, each associated with a particular realisation of the environmental noises $\{\mathrm{dW}_k\}$ [62], or equivalently, an initial environmental state. The ensemble-averaged density matrix $\bar{\rho}$ then corresponds to taking an average over the noise and hence over all possible trajectories and, as a result, equation (9) is recovered. If the system were closed instead of open, interactions between the system and the environment would vanish and we would be left with the first term on the right-hand side; namely the von Neumann equation. A similar stochastic evolution equation for $\rho$ has been derived by Jacobs by analogy with classical measurement theory [18]. Under this approach, however, the noise is interpreted as a quantum fluctuation stemming from the uncertainty in the measurement: a similar approach is taken by

Gambetta *et al* [27]. In contrast, we consider such a noise to reflect the probabilistic nature of interactions with an underspecified environment causing the quantum system to evolve in a stochastic manner.

## 3. System specification

### 3.1. SDE parameters

We consider a spin system with a Hamiltonian given by

$$H_s = \epsilon S_x, \tag{12}$$

where $\epsilon$ is a positive constant and the operator $S_x$ represents the $x$-component of the spin: for example in the case of a spin 1/2 system we have $S_i = \frac{1}{2}\sigma_i$ where $\sigma_i$ denotes a Pauli spin matrix. The spin operators satisfy the condition $[S_i, S_j] = i\epsilon_{ijk}S_k$ where $\epsilon_{ijk}$ is the Levi–Civita symbol. We shall consider cases of spin 1/2, spin 1 and spin 3/2 systems where the matrix representations of the $S_x$, $S_y$ and $S_z$ operators accordingly have dimensions 2, 3 and 4, respectively. The Hamiltonian in equation (12) produces Rabi oscillations, as we shall see.

The desired effect of the environment on the system is that it should act as a measuring apparatus. Diffusive evolution of the system's $z$-component of spin, to be defined shortly, towards one of the eigenstates of the $S_z$ operator, can be achieved using a single Lindblad operator in equation (11) of the form

$$L = \alpha S_z, \tag{13}$$

where the constant $\alpha$ denotes the degree of coupling between the system and its environment through the operator $S_z$ and can be regarded as the strength of measurement. Figure 1 illustrates the features of the system and its environment. Utilising the above expressions for the Lindblad operator and the system Hamiltonian in equation (11), the following SDE is obtained for the evolution of the reduced density matrix of the system:

$$\mathrm{d}\rho = -i\epsilon\,[S_x, \rho]\,\mathrm{d}t + \alpha^2\left(S_z\rho S_z - \frac{1}{2}\left(\rho S_z^2 + S_z^2\rho\right)\right)\mathrm{d}t + \alpha\left(\rho S_z + S_z\rho - 2\langle S_z\rangle\rho\right)\mathrm{dW}. \tag{14}$$

The single Wiener increment dW is a Gaussian noise with a mean of zero and a variance d$t$, and $\langle S_z\rangle$ is the $z$-component of spin, defined by $Tr(S_z\rho)$. Note that the latter is not to be confused with the usual quantum expectation value of $S_z$ which in our notation is $Tr(S_z\bar{\rho})$, where $\bar{\rho}(t)$ is the density matrix at time $t$ averaged over all possible quantum trajectories. The expectation value represents an average of a (projectively) measured system property taking into account the quantum mechanical randomness of measurement outcome as well as the range of quantum states that might be adopted by an open system when coupled to an uncertain environment. By extension, $\langle . \rangle = Tr(.\rho)$ could be interpreted as a conditional average projective measurement outcome given a specific stochastically evolving density matrix. But it could instead be regarded simply as a property of the density matrix, and hence of the physical state, and indeed it is spin components such as $\langle S_z\rangle$ that undergo Rabi oscillations.

Terms in equation (14) that depend on $\alpha$ represent the effects of measurement on the system, brought about by its interaction with the environment. Notice that for $\epsilon = 0$, the stationary states for the measurement dynamics are $\rho = |m_z\rangle\langle m_z|$, where the $|m_z\rangle$ are eigenstates of $S_z$ satisfying $S_z|m_z\rangle = m_z|m_z\rangle$. Starting from an arbitrary initial state, the coupling to the environment captured by the Lindblad operator in equation (13) evolves the system towards $z$-spin eigenstates as desired.

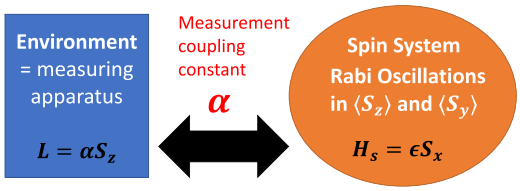


**Figure 1.** An open quantum spin system interacting with an environment with a strength defined by the coupling constant $\alpha$. The environment acts as a measurement apparatus, measuring the system's spin along the $z$-axis.

### *3.2. Density matrix parametrisation*

The density matrix of the open quantum system is to be parametrised by a set of variables $\{x_i\}$ which evolve stochastically according to the general Itô processes [63]:

$$\mathrm{d}x_i = A_i \mathrm{d}t + \sum_k B_{ik} \mathrm{dW}_k, \tag{15}$$

where $\mathrm{dW}_k$ denote the Wiener increments and the $A_i$ and $B_{ik}$ are designated functions. The number of parameters required to represent the density matrix depends on the system. Three are required for a density matrix describing a spin 1/2 system. For a spin 1 system, eight parameters are needed since this is the number of independent variables required to specify a $3 \times 3$ Hermitian matrix with unit trace. Through a similar reasoning, fifteen variables are needed to parametrise the density matrix for a spin 3/2 system.

*3.2.1. Spin 1/2.* The density matrix of a spin 1/2 system can be expressed using the Bloch sphere formalism, namely $\rho = \frac{1}{2}(\mathbb{I} + \boldsymbol{r}\cdot\boldsymbol{\sigma})$ with coherence (or Bloch) vector $\boldsymbol{r} = (x,y,z) = Tr(\rho\boldsymbol{\sigma}) = \langle\boldsymbol{\sigma}\rangle$ [64]. SDEs in the form of equation (15) can be derived starting from

$$\mathrm{d}r_i = Tr(\sigma_i \mathrm{d}\rho), \tag{16}$$

with the insertion of equation (14). For clarity of presentation, however, we shall employ a one parameter representation for the special case of a pure state with $Tr\rho^2 = 1$ or $|\boldsymbol{r}| = 1$, with coherence vector confined to the $(y,z)$ plane, i.e.

$$\rho = \frac{1}{2}(\mathbb{I} + \cos\phi\,\sigma_z - \sin\phi\,\sigma_y), \tag{17}$$

namely $x = 0$, $y = -\sin\phi$ and $z = \cos\phi$. The SDE for $z$ arising from $\mathrm{d}z = Tr(\sigma_z \mathrm{d}\rho)$ and equation (14) is

$$\mathrm{d}z = -\epsilon \sin\phi\,\mathrm{d}t + \alpha \sin^2\phi\,\mathrm{dW}. \tag{18}$$

The Rabi angle $\phi$ represents the angle of rotation of the coherence vector about the $x$ axis. In the absence of environmental coupling, the action of the system Hamiltonian $\frac{1}{2}\epsilon\sigma_x$ is to increase $\phi$ linearly in time. In the presence of such coupling the evolution of the Rabi angle represents the effect of measurement on the unitary dynamics of the system. The SDE for $\phi = \cos^{-1} z$ can be found through use of Itô's lemma [63]:

$$\mathrm{d}\phi = \frac{\mathrm{d}\phi}{\mathrm{d}z}\mathrm{d}z + \frac{1}{2}\beta^2 \frac{\mathrm{d}^2\phi}{\mathrm{d}z^2}\mathrm{d}t, \tag{19}$$

where $\beta = \alpha \sin^2\phi$. Inserting equation (18) produces

$$\mathrm{d}\phi = \left(\epsilon - \frac{1}{4}\alpha^2 \sin 2\phi\right)\mathrm{d}t - \alpha \sin\phi \,\mathrm{dW}. \tag{20}$$

When $\alpha = 0$ the Rabi angle increases at a constant rate, while for $\alpha \neq 0$ the Wiener noise dW disturbs its evolution. The average rate of change of $\phi$ is given by

$$\frac{\mathrm{d}\langle\phi\rangle}{\mathrm{d}t} = \epsilon - \frac{1}{4}\alpha^2\langle \sin 2\phi\rangle, \tag{21}$$

where the brackets again represent an ensemble average. The QZE will emerge if the term proportional to $\alpha^2$ represents an average retardation of the rotation. In order to resolve this matter we consider the Fokker–Planck equation for $p(\phi, t)$, the probability distribution function (PDF) of the Rabi angle $\phi$:

$$\frac{\partial p}{\partial t} = -\frac{\partial\left(\left(\epsilon - \frac{1}{4}\alpha^2 \sin 2\phi\right)p\right)}{\partial\phi} + \frac{1}{2}\alpha^2\frac{\partial^2\left(\sin^2\phi\, p\right)}{\partial\phi^2}. \tag{22}$$

For small $\alpha$, an approximate stationary PDF may be obtained:

$$p_{st}(\phi) \propto 1 + \frac{3\alpha^2}{4\epsilon}\sin 2\phi, \tag{23}$$

which shows that the PDF is disturbed from uniformity, in this regime, by increasing the environmental coupling $\alpha$, or by reducing $\epsilon$ and hence slowing the rate of Rabi oscillation for an isolated system. We shall investigate the shape of the stationary PDF numerically for a range of $\alpha$ in section 4. For now, let us notice that using this approximation the average needed in equation (21) is proportional to

$$\int_0^{2\pi}\mathrm{d}\phi\left(1 + \frac{3\alpha^2}{4\epsilon}\sin 2\phi\right)\sin 2\phi \propto \int_0^{2\pi}\mathrm{d}\phi \sin^2 2\phi > 0, \tag{24}$$

showing that the effect of measurement at small $\alpha$ is indeed a mean retardation of the Rabi oscillations, consistent with the quantum Zeno effect.

*3.2.2. Spin 1.* The generalised Bloch sphere formalism is used to represent the density matrix of a spin 1 system. This permits any $3 \times 3$ density matrix to be written in terms of the Gell–Mann matrices $\lambda_i$ through

$$\rho = \frac{1}{3}\left(\mathbb{I} + \sqrt{3}\boldsymbol{R}\cdot\boldsymbol{\lambda}\right), \tag{25}$$

where $\boldsymbol{R} = (s, m, u, v, k, x, y, z)$ is an eight dimensional coherence (or Bloch) vector and the Gell–Mann matrices (see appendix A) form the elements of the vector $\boldsymbol{\lambda} = (\lambda_1, \lambda_2, \lambda_3, \lambda_4, \lambda_5, \lambda_6, \lambda_7, \lambda_8)$ [65]. The following density matrix emerges for the spin 1 system:

$$\rho = \frac{1}{3}\begin{pmatrix} 1 + \sqrt{3}u + z & -i\sqrt{3}m + \sqrt{3}s & \sqrt{3}v - i\sqrt{3}k \\ i\sqrt{3}m + \sqrt{3}s & 1 - \sqrt{3}u + z & \sqrt{3}x - i\sqrt{3}y \\ \sqrt{3}v + i\sqrt{3}k & \sqrt{3}x + i\sqrt{3}y & 1 - 2z \end{pmatrix}. \tag{26}$$

Stochastic quantum trajectories can be produced from the equations of motion for the eight variables parametrising $\rho$. As before, these are generated from

$$\mathrm{d}R_i = \frac{\sqrt{3}}{2} Tr\left(\mathrm{d}\rho\lambda_i\right), \tag{27}$$

using the properties of the Gell–Mann matrices, and are specified in appendix B. The components of the coherence vector $\boldsymbol{R}$ are denoted $R_i$.

*3.2.3. Spin 3/2.* In order to construct the density matrix of the spin 3/2 system, an obvious representation would be to utilise SU(4) generators in the generalised Bloch sphere representation:

$$\rho = \frac{1}{4}\left(\mathbb{I} + \boldsymbol{s}\cdot\boldsymbol{\Sigma}\right). \tag{28}$$

The 15 component coherence vector is $\boldsymbol{s} = (v,e,f,g,h,j,k,l,m,n,o,p,q,s,u)$ and the vector of generators $\boldsymbol{\Sigma}$ has components $\Sigma_k$ with $k = 1,15$. However, Aerts and Sassoli de Bianchi discuss how such a representation beyond the SU(2) generators could potentially allow the system to explore unphysical states [64]. Instead, we use equation (28) with generators $\Sigma_k$ constructed using the tensor product of two Pauli matrices: $\Sigma_k = \sigma_i \otimes \sigma_j$: full details are given in appendix C. The following density matrix is then obtained for the spin 3/2 system:

$$\rho = \frac{1}{4}\begin{pmatrix} 1+f+p+u & -ie+q-is+v & g+k-il-io & h-ij-im-n \\ ie+q+is+v & 1-f+p-u & h+ij-im+n & g-k-il+io \\ g+k+il+io & h-ij+im+n & 1+f-p-u & -ie-q+is+v \\ h+ij+im-n & g-k+il-io & ie-q-is+v & 1-f-p+u \end{pmatrix}. \tag{29}$$

As before, stochastic quantum trajectories can be produced from the equations of motion of the 15 variables parametrising the density matrix. SDEs for components of the coherence vector $s_k$ are obtained through

$$\mathrm{d}s_k = Tr\left(\mathrm{d}\rho\Sigma_k\right), \tag{30}$$

and the details can be found in appendix D.

### *3.3. Spin component SDEs*

The stochastic trajectories of the variables parametrising the density matrices introduced for the spin quantum systems enable us to describe the system dynamics exactly, but do not offer much direct physical insight into the QZE. A more useful way of visualising the behaviour of such systems is to consider the evolution of the time dependent quantities $\langle S_x\rangle$, $\langle S_y\rangle$ and $\langle S_z\rangle$. Recall that these could be interpreted as conditional average values under projective measurements, hence a set of statistics of the dynamics, though we prefer to regard them as actual physical properties of the current quantum state. It is these quantities that perform noisy Rabi oscillations and we shall refer to them simply as spin components. Two methods exist to determine their evolution.

The first method simply employs $\langle S_i\rangle = Tr(S_i\rho)$ such that the spin components can be written in terms of the variables parametrising the density matrices in equations (17), (26) and (29). Alternatively, by considering $\mathrm{d}\langle X\rangle = Tr(X\mathrm{d}\rho)$, where operators $X$ are various functions of the $S_i$, the SDEs that govern the evolution of the spin components can be found using equation (14) and solved. We consider these approaches for the three spin systems in turn.

*3.3.1. Spin 1/2.* For the special case density matrix in equation (17) the spin components $\langle S_y\rangle$ and $\langle S_z\rangle$ can be written in terms of the Rabi angle $\phi(t)$ as follows:

$$\langle S_y\rangle = -\frac{1}{2}\sin\phi, \qquad \langle S_z\rangle = \frac{1}{2}\cos\phi, \tag{31}$$

so the phase space explored by $\langle S_y\rangle$ and $\langle S_z\rangle$ is a circle of radius $1/2$. We expect a typical stochastic trajectory to dwell increasingly in the vicinity of the $z$-spin eigenstates at $\phi = 0$ and $\pi$ as the measurement strength increases, and will demonstrate this in section 4. We also expect the mean rate of passage between the two eigenstates to reduce as the measurement strength increases.

The following three SDEs describe the spin components:

$$\begin{aligned}
\mathrm{d}\langle S_z\rangle &= \epsilon\langle S_y\rangle \mathrm{d}t + 2\alpha\left(\frac{1}{4} - \langle S_z\rangle^2\right)\mathrm{dW}\\
\mathrm{d}\langle S_x\rangle &= -\frac{\alpha^2}{2}\langle S_x\rangle \mathrm{d}t - 2\alpha\langle S_z\rangle\langle S_x\rangle \mathrm{dW}\\
\mathrm{d}\langle S_y\rangle &= -\epsilon\langle S_z\rangle \mathrm{d}t - \frac{\alpha^2}{2}\langle S_y\rangle \mathrm{d}t - 2\alpha\langle S_z\rangle\langle S_y\rangle \mathrm{dW}.
\end{aligned} \tag{32}$$

For $\alpha = 0$ we clearly see the emergence of Rabi oscillations in $\langle S_y\rangle$ and $\langle S_z\rangle$. Similarly, for $\epsilon = 0$ we identify stationary states at $\langle S_x\rangle = \langle S_y\rangle = 0$ and $\langle S_z\rangle = \pm 1/2$, which correspond to the measurement eigenstates.

It may be shown that the purity of the system defined by $P = Tr(\rho^2)$ satisfies

$$\mathrm{d}P = \alpha^2\left(1 - r_z^2\right)(1-P)\,\mathrm{d}t + 2\alpha r_z(1-P)\,\mathrm{dW}, \tag{33}$$

such that purity moves towards $P = 1$ and stays there under the given dynamics. Furthermore, $\langle S_x\rangle = 0$ is a fixed point of the dynamics of equation (32) so the special case considered in equation (17) describes a more general asymptotic behaviour.

*3.3.2. Spin 1.* Similarly, the spin components $\langle S_x\rangle$, $\langle S_y\rangle$ and $\langle S_z\rangle$ can be written in terms of the variables parametrising the density matrix in equation (26):

$$\begin{aligned}
\langle S_x\rangle &= \sqrt{\frac{2}{3}}(x+s)\\
\langle S_y\rangle &= \sqrt{\frac{2}{3}}(m+y)\\
\langle S_z\rangle &= \frac{u}{\sqrt{3}} + z.
\end{aligned} \tag{34}$$

The purity $P$ of the system can be written

$$P = Tr\left(\rho^2\right) = \frac{2}{3}\left(s^2+m^2+u^2+v^2+k^2+x^2+y^2+z^2\right) + \frac{1}{3}, \tag{35}$$

and this evolves asymptotically to unity. The dynamics in terms of spin components and related quantities take the form of eight coupled SDEs:

$$
\begin{aligned}
\mathrm{d}\langle S_z\rangle &= \epsilon\langle S_y\rangle \mathrm{d}t + 2\alpha\left(\langle S_z^2\rangle - \langle S_z\rangle^2\right)\mathrm{dW}\\
\mathrm{d}\langle S_x\rangle &= -\frac{\alpha^2}{2}\langle S_x\rangle \mathrm{d}t + \alpha\left(\langle S_z S_x\rangle + \langle S_x S_z\rangle - 2\langle S_z\rangle\langle S_x\rangle\right)\mathrm{dW}\\
\mathrm{d}\langle S_y\rangle &= -\epsilon\langle S_z\rangle \mathrm{d}t - \frac{\alpha^2}{2}\langle S_y\rangle \mathrm{d}t + \alpha\left(\langle S_z S_y\rangle + \langle S_y S_z\rangle - 2\langle S_z\rangle\langle S_y\rangle\right)\mathrm{dW}\\
\mathrm{d}\langle S_y^2\rangle &= -\epsilon\left(\langle S_y S_z\rangle + \langle S_z S_y\rangle\right)\mathrm{d}t - \alpha^2\left(i\langle S_x S_y S_z\rangle + \langle S_z^2\rangle + \langle S_y^2\rangle - 1\right)dt\\
&\quad + \alpha\langle S_z\rangle\left(1 - 2\langle S_y^2\rangle\right)\mathrm{dW}\\
\mathrm{d}\langle S_z^2\rangle &= \epsilon\left(\langle S_y S_z\rangle + \langle S_z S_y\rangle\right)\mathrm{d}t + 2\alpha\langle S_z\rangle\left(1 - \langle S_z^2\rangle\right)\mathrm{dW}\\
\mathrm{d}\left(\langle S_y S_z\rangle + \langle S_z S_y\rangle\right) &= 2\epsilon\left(\langle S_y^2\rangle - \langle S_z^2\rangle\right)\mathrm{d}t - \frac{\alpha^2}{2}\left(\langle S_y S_z\rangle + \langle S_z S_y\rangle\right)\mathrm{d}t\\
&\quad + \alpha\left(\langle S_y\rangle - 2\langle S_z\rangle\left(\langle S_y S_z\rangle + \langle S_z S_y\rangle\right)\right)\mathrm{dW}\\
\mathrm{d}\left(\langle S_z S_x\rangle + \langle S_x S_z\rangle\right) &= -\frac{\alpha^2}{2}\left(\langle S_x S_z\rangle + \langle S_z S_x\rangle\right)\mathrm{d}t + \alpha\left(\langle S_x\rangle - 2\langle S_z\rangle\left(\langle S_x S_z\rangle + \langle S_z S_x\rangle\right)\right)\mathrm{dW}\\
\mathrm{d}\langle S_x S_y S_z\rangle &= i\epsilon\left(\langle S_y S_z\rangle + \langle S_z S_y\rangle\right)\mathrm{d}t + i\alpha^2\left(\langle S_z^2\rangle + 2i\langle S_x S_y S_z\rangle\right)\mathrm{d}t\\
&\quad + i\alpha\langle S_z\rangle\left(1 + 2i\langle S_x S_y S_z\rangle\right)\mathrm{dW}.
\end{aligned}
\tag{36}
$$

Again, the regular Rabi dynamics around a circle in the phase space spanned by $\langle S_y\rangle$ and $\langle S_z\rangle$ is apparent when $\alpha = 0$. When $\alpha \neq 0$ the trajectories are more complicated. For $\epsilon = 0$ the eigenstates of the $z$-spin are stationary: the relevant spin components being $\langle S_x\rangle = \langle S_y\rangle = 0$ and $\langle S_z\rangle = \pm 1, 0$.

*3.3.3. Spin 3/2.* Once again, the spin components can be written in terms of the variables parametrising the density matrix for the spin 3/2 system in equation (29) as follows:

$$
\begin{aligned}
\langle S_x\rangle &= \frac{1}{2}\left(h + n + \sqrt{3}v\right)\\
\langle S_y\rangle &= \frac{1}{2}\left(\sqrt{3}e - j + m\right)\\
\langle S_z\rangle &= \frac{1}{2}f + p.
\end{aligned}
\tag{37}
$$

The purity of the system $P$ may be written

$$
P = \frac{1}{4}\left(1 + e^2 + f^2 + g^2 + h^2 + j^2 + k^2 + l^2 + m^2 + n^2 + o^2 + p^2 + q^2 + s^2 + u^2 + v^2\right). \tag{38}
$$

For the spin 3/2 system a closed set of fifteen stochastic differential equations for the spin components and related quantities could not be found. Thus equation (37) and the SDEs in appendix D are the only way to solve the dynamics for this spin system.

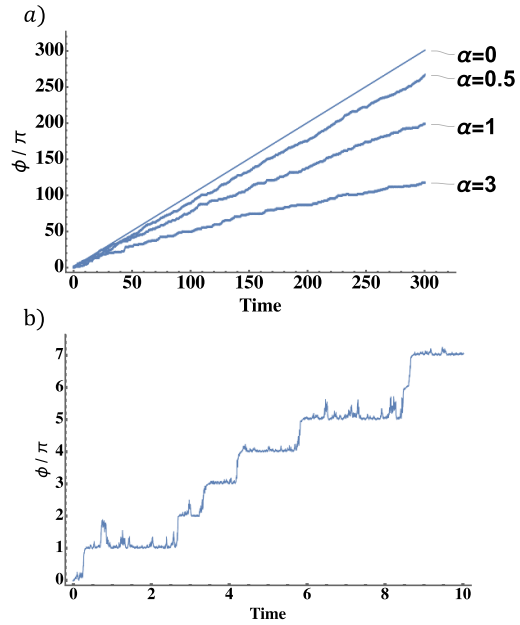


**Figure 2.** (a) The evolution of the Rabi angle $\phi$ for a spin 1/2 system at four values of $\alpha$ with time-step 0.0005, $\epsilon = 1$ and a duration of 300 time units. The mean rate of change is reduced as the strength of measurement is increased. (b) Close-up of the evolution of $\phi$ for $\alpha = 1$ for a duration of 10 time units. Notice that for this strength of measurement the Rabi angle tends to dwell in the vicinity of integer multiples of $\pi$, the $z$-spin eigenstates.

## 4. Simulations and results

### *4.1. Spin 1/2*

The equations of motion for the variables parametrising the density matrices of the spin 1/2, spin 1 and spin 3/2 systems, given by equations (20), (27) and (30), were solved numerically using the Euler-Maruyama update method [66]. From the evolution of these variables, stochastic quantum trajectories in the phase space of the $z$-spin component $\langle S_z \rangle$ and the $y$-spin component $\langle S_y \rangle$ were produced. For spin 1/2 we also generated stochastic trajectories of the Rabi angle $\phi$. We chose the $x$-spin component to be zero initially, where it remains.

The evolution of the Rabi angle with time for the spin 1/2 system for various strengths of measurement is shown in figure 2. Figure 2(a) shows that the mean rate of change of the Rabi angle, namely the mean frequency of Rabi oscillations, decreases with increasing measurement coupling constant, as was suggested by equation (21). Such a decrease demonstrates the slowing down of the unitary dynamics as a result of stronger, or equivalently, more frequent measurement as is expected for the QZE. Figure 2(b) illustrates the dynamics on a finer scale. Behaviour at high measurement strength resembles the quantum jumps conventionally considered to occur between eigenstates of a monitored observable, brought about by an interaction present in the Hamiltonian.

Numerically generated stationary PDFs for the Rabi angle are shown in figure 3 for an isolated system ($\alpha = 0$) and for three nonzero measurement strengths. Initial states were selected from a uniform probability density over $\phi$. Angles $\phi = 0$ and $\pi$ correspond to the $|\frac{1}{2}\rangle$ and $|-\frac{1}{2}\rangle$ eigenstates of $S_z$, respectively. Values of $\phi$ from the trajectories are mapped into the range 0 to

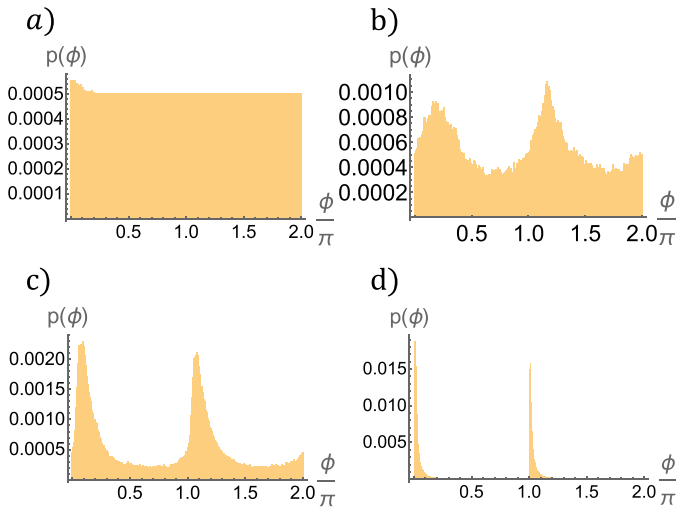


**Figure 3.** Stationary probability density functions for the Rabi angle in the spin 1/2 system, for a range of measurement strengths $\alpha$, obtained over a duration of 300 time units with a time-step of 0.0005 and $\epsilon = 1$. (a) $\alpha = 0$, (b) $\alpha = 0.5$, (c) $\alpha = 1$, (d) $\alpha = 3$. The eigenstates of $S_z$ lie at $\phi = 0$ and at $\phi = \pi$. Notice the displacement of the peaks above the eigenvalues, arising from the rotational pull of the system Hamiltonian.

$2\pi$. It can be seen that as the measurement strength is increased, the stationary PDFs become narrower since the measurement dynamics are better able to localise the system in the vicinity of the eigenstates of $S_z$, resisting the pull of the unitary dynamics induced by the Hamiltonian, which seek to drive the system into Rabi oscillations. In accordance with the Born rule, for $\alpha > 0$ the stationary PDFs contain two approximately equivalent peaks around the $|-\frac{1}{2}\rangle$ and $|\frac{1}{2}\rangle$ eigenstates, since the system should have an equal probability of localising at either. The PDF in figure 3(a) is uniform over $\phi$ since the trajectories represent the dynamics without measurement, namely Rabi oscillations. Note that the stationary PDF in figure 3(b) is roughly sinusoidal, as suggested by the PDF for small $\alpha$ given in equation (23). Indeed, that approximate result suggested peaks at $\phi = \pi/4$ and $3\pi/4$: a consequence of the competition between measurement-induced dwell near the eigenstates and the rotational pull of the Hamiltonian. As measurement strength increases, the peaks are drawn closer to $\phi = 0$ and $\pi$.

### *4.2. Spin 1*

The evolution of $\langle S_z \rangle$ and $\langle S_y \rangle$ for a spin 1 system, for different values of the measurement strength $\alpha$, is illustrated in figure 4. The system was initialised in the $|-1\rangle$ spin eigenstate of the $S_z$ operator. Figure 4(a) illustrates the dynamics when there is no measurement: the Hamiltonian drives Rabi oscillations in $\langle S_z \rangle$ and $\langle S_y \rangle$ corresponding to the precession of the spin vector around the orthogonal $\langle S_x \rangle$ axis. The $|\pm 1\rangle$ and $|0\rangle$ eigenstates of $S_z$ lie at $\langle S_x \rangle = 0$, $\langle S_y \rangle = 0$ and $\langle S_z \rangle = \pm 1$ and 0, respectively. If the initial state of the system had been the $|0\rangle$ eigenstate of $S_z$, then the spin vector would lie on the $\langle S_x \rangle$ axis and would be unable to precess around it, and furthermore, $\langle S_z \rangle$ and $\langle S_y \rangle$ would be zero.

Disturbance of the circular trajectories can be seen in figure 4(b). As a result of the non-zero measurement strength the system can now pass near the $|0\rangle$ eigenstate of $S_z$, located at the origin. As the $\alpha$ is increased further in figures 4(c), (d), a figure-of-eight pathway forms

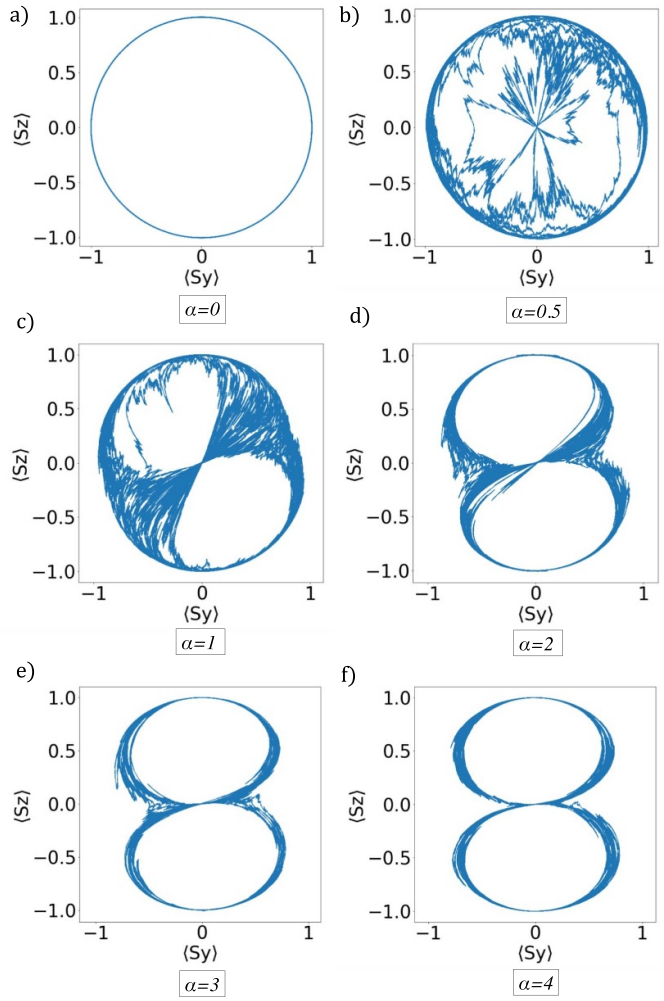


**Figure 4.** The path taken through $\langle S_y \rangle$, $\langle S_z \rangle$ phase space for a spin 1 system with varying measurement strength $\alpha$, for $\epsilon = 1$, time-step 0.0001 and for a duration of 50 time units. As $\alpha$ increases, the circular path corresponding to regular Rabi oscillations at $\alpha = 0$ becomes disturbed, allowing visits to the $|0\rangle$ eigenstate at the origin in addition to the $|\pm 1\rangle$ eigenstates at the top and bottom of the phase space.

and the system dwells more often at the $|0\rangle$ eigenstate until, in figures 4(e), (f), visits to this state always occur in between visits to the $|-1\rangle$ and $|1\rangle$ eigenstates.

Note that the spin 1 system is not moving at a constant speed around these figure-of-eight pathways. Instead, the system makes rapid jumps between the eigenstates, typically in a counter-clockwise direction, separating periods of dwell in the vicinity of the eigenstates. Movies of examples of the spin 1 [67] and spin 3/2 [68] system dynamics are available. The behaviour is illustrated in plots of the relative probability of occupation of patches of the phase space by the system, shown in figure 5. The behaviour is similar to that of the spin 1/2 system: a greater tendency to localise near the eigenstates as $\alpha$ is increased, while the pull of the Hamiltonian produces a counterclockwise displacement.

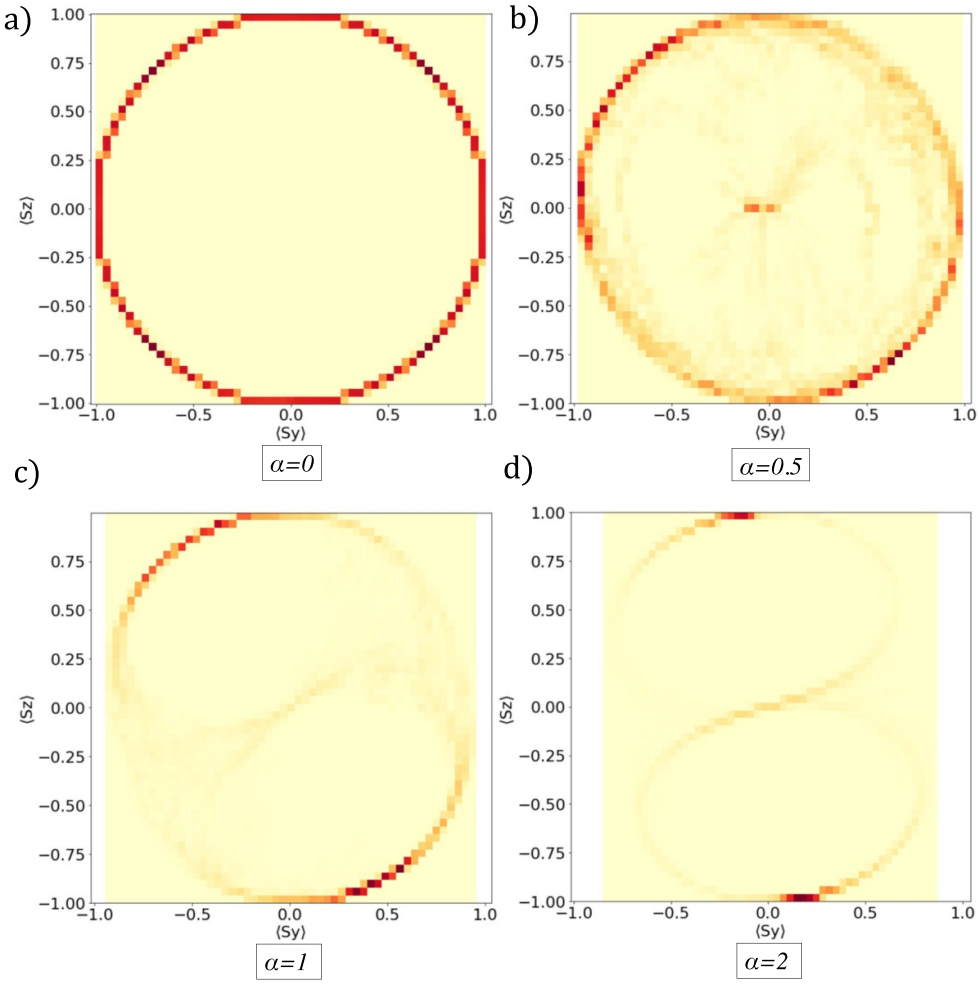


**Figure 5.** Density plot (51 by 51 bins) illustrating stationary relative occupation in the $\langle S_y \rangle, \langle S_z \rangle$ phase space of the spin 1 system for four values of $\alpha$, obtained from trajectories with a duration of 100 time units, a time-step of 0.0001 and $\epsilon = 1$.

Figure 6 further illustrates how increasing the measurement coupling constant causes the system to dwell for longer at the three eigenstates of $S_z$ and transit more abruptly between them. The behaviour at high measurement strength increasingly resembles the textbook behaviour of a system making jumps between eigenstates.

In order to quantify the QZE, we consider the $\alpha$ dependence of two quantities derived from the trajectories in figure 4. First, the residence probabilities, which characterise the fraction of time spent in the vicinity of each eigenstate of $S_z$ over a long simulation. The system is defined to occupy an eigenstate if the $\langle S_z \rangle$ coordinate lies within $\pm$ 0.1 of the appropriate eigenvalue. The second quantity considered is the mean return time. This is the average period from the moment the system leaves a particular eigenstate (with occupation defined as above) to the moment it returns to it having visited another eigenstate in between.

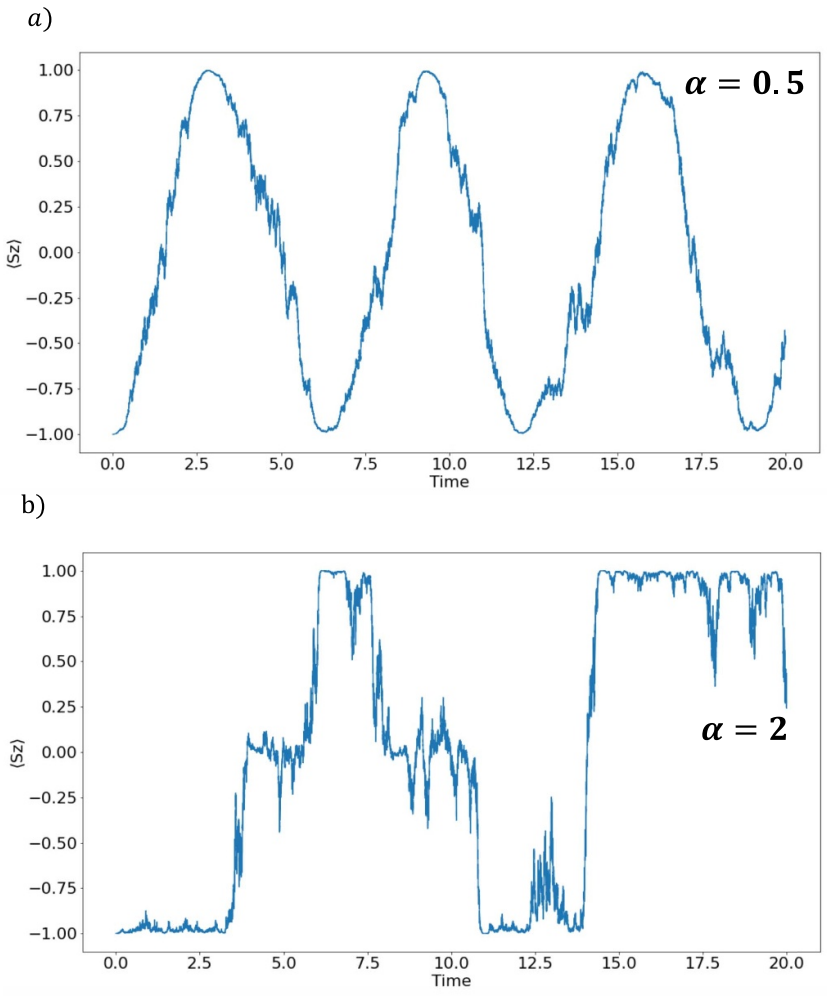


**Figure 6.** Trajectories of $\langle S_z \rangle$ for the spin 1 system for (a) $\alpha = 0.5$ and (b) $\alpha = 2$. Slightly noisy Rabi oscillations at low measurement strength are contrasted with fast jumps between the eigenstates at $\langle S_z \rangle = \pm 1$ and 0, with random waiting times, when the measurement strength is increased.

Figure 7(a) illustrates how residence probabilities are small for low values of $\alpha$, which is a reflection of the only slightly disturbed oscillatory behaviour of $\langle S_z \rangle$ in figure 6(a). But as the coupling strength is raised, so do the residence probabilities, and this can similarly be understood by considering the trajectory shown in figure 6(b). Little time is spent in regions far away from the eigenstates. Visits to the $\langle S_z \rangle = 0$ eigenstate are less frequent than to the $\pm 1$ eigenstates for small $\alpha$, which is a consequence of having started the trajectory at $\langle S_z \rangle = -1$, but they occur with approximately equal probability at high values of $\alpha$.

Figure 7(b) shows how the system takes longer times to return to an eigenstate for stronger measurement. Again, this is consistent with the behaviour shown in figure 6(b). The mean return time for a given eigenstate is dominated by the period of dwell at the eigenstate (or eigenstates) to which it moves. The mean return time to the $\langle S_z \rangle = 0$ state initially decreases

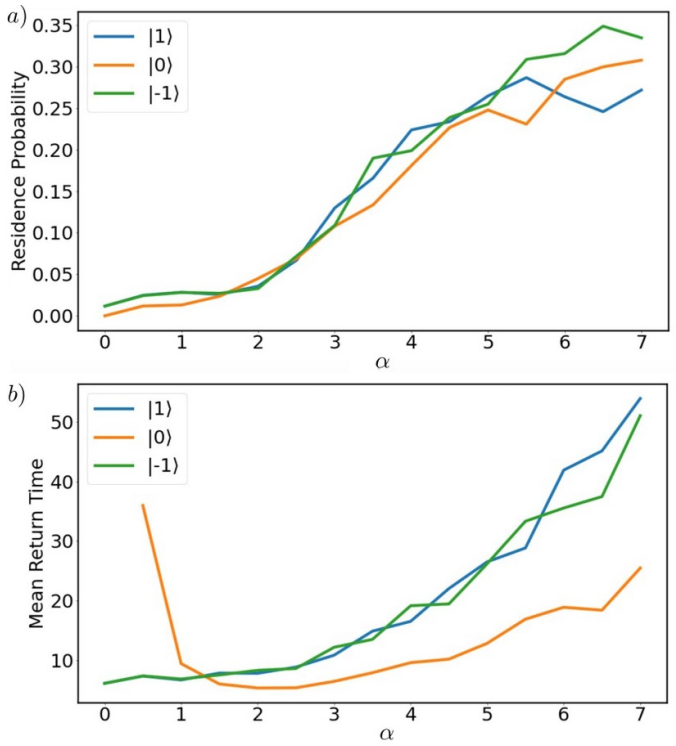


**Figure 7.** Colour. (a) Residence probabilities, and (b) mean return times for the eigenstates of a spin 1 system, with varying measurement strength $\alpha$, for $\epsilon = 1$, time-step of 0.0001 and for a duration of 5000 time units.

with $\alpha$ but this is an artefact of the initial condition for the motion, which makes visits to this eigenstate rare when $\alpha$ is small (as is apparent in figure 4). The mean return time for the $\langle S_z \rangle = 0$ eigenstate is typically less than the return times for $\langle S_z \rangle = \pm 1$ (roughly half), possibly because direct transitions between the $\langle S_z \rangle = 1$ and $-1$ states are unlikely. Return to the central eigenstate is characterised by just one period of dwell at one of the two outer eigenstates, while return to an outer eigenstate might require waiting while the system hops between the other two states. The mean return times in figure 6(b) can be compared to the average time between two jumps $\tau$ found from the analytical expression of the jump rates in Bauer *et al* [34]. Specifically, for $\alpha = 7$, the average time between two jumps for the $|\pm 1\rangle$ eigenstates is $\tau_{|\pm 1\rangle} = 49$ and for the $|0\rangle$ eigenstate is $\tau_{|0\rangle} = 24.5$, showing good agreement with our results.

The definition of the vicinity of an eigenstate is, of course, open to debate. The choice we make is simple but is sufficient to reveal the effects that characterise the QZE. It is natural that the value of $\langle S_z \rangle$ should feature prominently in the definition, but there are other characteristics of the eigenstates that could be taken into account. An eigenstate of the $S_z$ operator corresponds to a point in a multidimensional parameter space, and its vicinity could be defined by putting conditions on a variety of parameters. We have investigated a more elaborate scheme along these lines but the resulting residence probabilities and mean return times are broadly similar to those shown in figure 7. In the interests of simplicity we therefore focus on the value of $\langle S_z \rangle$ alone, and the chosen range of $\pm 0.1$ about eigenvalues.

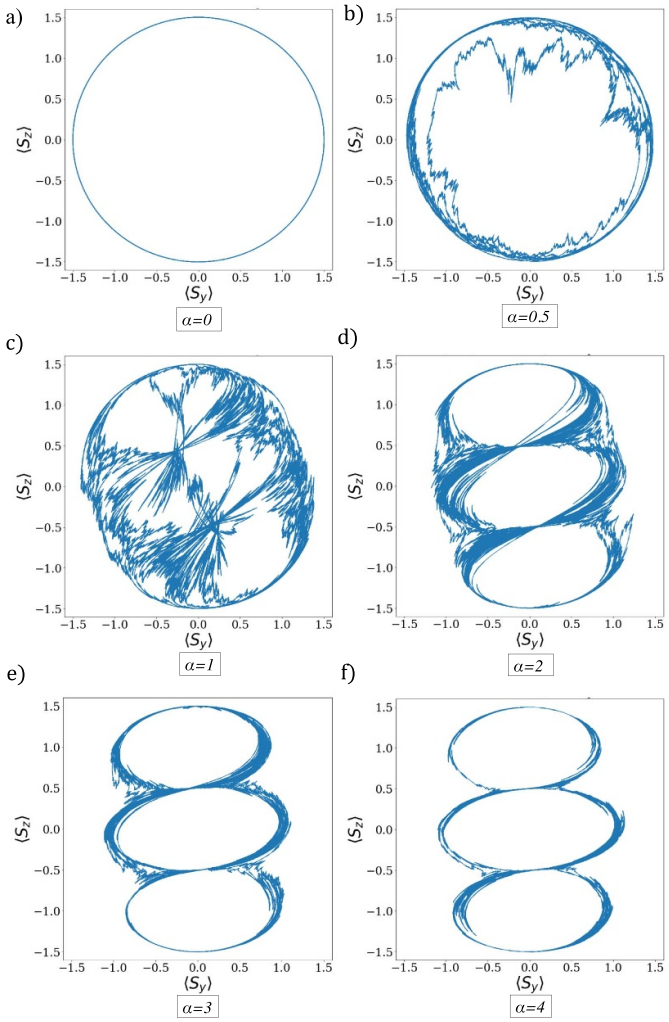


**Figure 8.** Paths through the $\langle S_y\rangle$, $\langle S_z\rangle$ phase space explored by a spin 3/2 system with varying measurement strength $\alpha$, for $\epsilon = 1$, time-step 0.0001 and duration 50 time units.

### *4.3. Spin 3/2*

The effects of measurement on a spin 3/2 system, viewed in terms of the evolution of spin components $\langle S_z\rangle$ and $\langle S_y\rangle$, is illustrated in figure 8 for different values of the measurement strength $\alpha$. The system was initialised in the $|-\frac{3}{2}\rangle$ eigenstate of $S_z$. When $\alpha = 0$ there is no measurement and, as with the spin 1 system, the Hamiltonian drives circular trajectories, as depicted in figure 8(a), passing through the $|\frac{3}{2}\rangle$ and $|-\frac{3}{2}\rangle$ eigenstates of $S_z$ at $\langle S_y\rangle = 0$ and $\langle S_z\rangle = \pm 3/2$. The spin vector processes around the $\langle S_x\rangle$ axis. As $\alpha$ is increased (figures 8(b)–(f)), the circular trajectory is disturbed such that the system passes through further regions of phase space, including the vicinities of the $|\frac{1}{2}\rangle$ and $|-\frac{1}{2}\rangle$ eigenstates of $S_z$ at $\langle S_y\rangle = 0$ and $\langle S_z\rangle = \pm 1/2$.

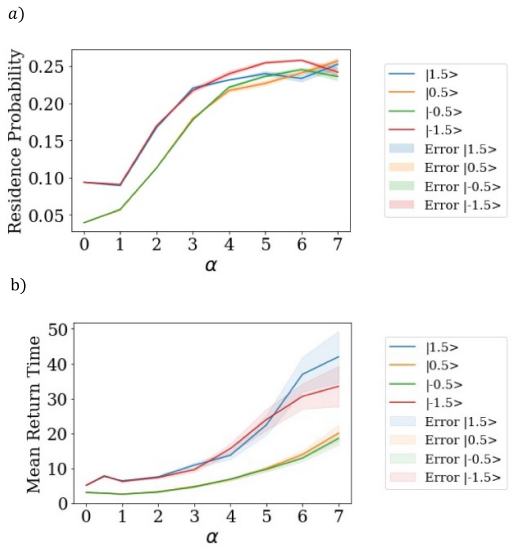


**Figure 9.** Color. The residence probabilities and mean return times for the eigenstates of a spin 3/2 system, with varying measurement strength $\alpha$, for $\epsilon = 1$, time-step of 0.0001 and for a duration of 5000 time units.

When the measurement strength is sufficiently high, a triple figure-of-eight trajectory emerges, such that the $|\frac{1}{2}\rangle$ and $|-\frac{1}{2}\rangle$ eigenstates are encountered between visits to the $|\frac{3}{2}\rangle$ eigenstate and the $|-\frac{3}{2}\rangle$ eigenstate, and visa-versa. The system dwells in the vicinities of all four eigenstates of $S_z$ for high enough $\alpha$.

Similarly to the spin 1 case, figure 11 reveals how increasing $\alpha$ leads to longer dwell at the eigenstates of $S_z$ and more 'jump-like' behaviour in between.

Figure 9(a) illustrates how the residence probabilities for the spin 3/2 system depend on $\alpha$. As with the spin 1 case, the system is defined to occupy an eigenstate if the $\langle S_z \rangle$ coordinate lies within $\pm 0.1$ of the appropriate eigenvalue. At low values of $\alpha$, the Hamiltonian term dominates and therefore occupation of the $|\frac{1}{2}\rangle$ and $|-\frac{1}{2}\rangle$ eigenstates of $S_z$ is lower than for the $|\frac{3}{2}\rangle$ and $|-\frac{3}{2}\rangle$ eigenstates. For higher values of $\alpha$, the residence probabilities for all four eigenstates increase and become roughly equal, in concord with the Born rule, and a triple figure-of-eight trajectory is followed. For large $\alpha$, the probability of occupying each eigenstate lies around 0.25, implying that the system is unlikely to occupy a point in the phase space outside the vicinity of the eigenstates. Note that increasing the value of $\alpha$ amplifies the noise term in equation (14), introducing greater statistical uncertainty into the simulation.

Figure 9(b) shows that as the measurement coupling constant is raised the mean return times increase, hence demonstrating the QZE. Notably, the mean return times for the $|\frac{1}{2}\rangle$ and $|-\frac{1}{2}\rangle$ eigenstates of $S_z$ are approximately half those of the $|\frac{3}{2}\rangle$ and $|-\frac{3}{2}\rangle$ eigenstates. When the system resides at the $|\frac{1}{2}\rangle$ and $|-\frac{1}{2}\rangle$ eigenstates, and $\alpha$ is high enough, there are two states to which it can transfer, as opposed to one when it resides at the $|\frac{3}{2}\rangle$ and $|-\frac{3}{2}\rangle$ eigenstates. The $|\pm\frac{1}{2}\rangle$ lie within the ladder of eigenstates while the $|\pm\frac{3}{2}\rangle$ are its termini. Twice the number of paths for a return to $|\frac{1}{2}\rangle$ compared with $|\frac{3}{2}\rangle$ suggests half the mean return time. The analytical average

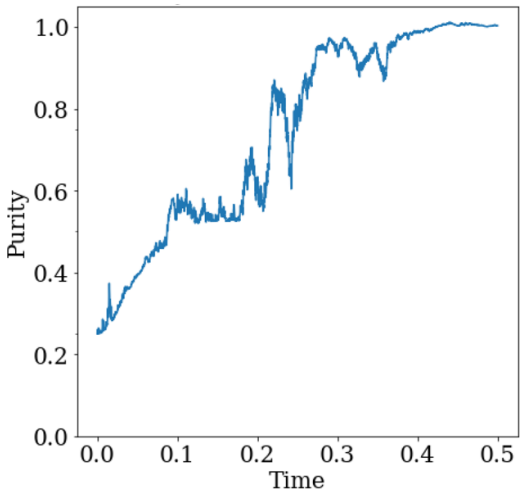


**Figure 10.** The evolving purity of a spin 3/2 system for a single quantum trajectory, starting from a fully mixed state, with $\alpha = 3$, $\epsilon = 1$, time-step 0.0001 and for a duration of 0.5 time units.

time between two jumps $\tau$, found from the analytical jump rates in Bauer *et al,* also reflect this trend. Namely, for $\alpha = 7$, the average time between two jumps for the $|\pm\frac{3}{2}\rangle$ eigenstates is $\tau_{|\pm\frac{3}{2}\rangle} \approx 32.7$ and for the $|\pm\frac{1}{2}\rangle$ eigenstates is $\tau_{|\pm\frac{1}{2}\rangle} = 14$ [34].

We speculate that higher spin systems will continue this pattern of behaviour. Systems with large measurement strength will follow stochastic transitions along a multiple figure-of-eight pathway in the phase space of $\langle S_z\rangle$ and $\langle S_y\rangle$. The behaviour will evolve from regular Rabi oscillations towards a situation where the system (effectively) jumps stochastically between eigenstates of the monitored observable.

Finally, the evolution of the purity of the spin 3/2 system under measurement was studied to ensure it remained within the expected range of $\frac{1}{4} \leqslant P \leqslant 1$, starting with the system in the fully mixed state $\rho = \frac{1}{4}\left(|-\frac{3}{2}\rangle\langle-\frac{3}{2}| + |-\frac{1}{2}\rangle\langle-\frac{1}{2}| + |\frac{1}{2}\rangle\langle\frac{1}{2}| + |\frac{3}{2}\rangle\langle\frac{3}{2}|\right)$. In figure 10 it can be seen that the effect of measurement is to cause the system to purify. The purification occurs in a continuous but stochastic manner, taking approximately 0.4 time units for the parameters chosen. The approximation of instantaneous projective measurements and apparent jumps in purity emerges only in the limit $\alpha \to \infty$.

It is worth noting that the dynamical framework we use has the effect that interaction brings about a *disentanglement* of the system from its environment, namely an increase in purity, which is the opposite of what is often supposed. However, this is an appropriate outcome for measurement, where the idea is to convey the system into a (pure) eigenstate of the appropriate observable. More general system-environment interactions might change the system purity in different ways, but to take this into account would require a more explicit representation of environmental degrees of freedom than that which we have employed.

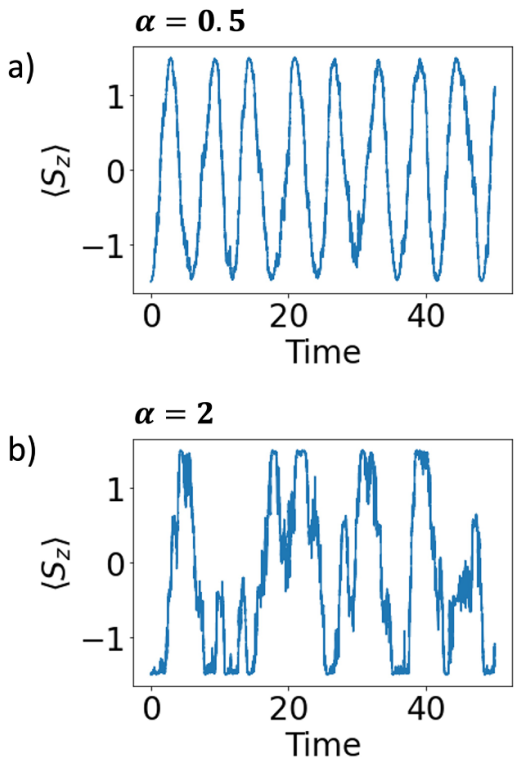


**Figure 11.** Trajectories of $\langle S_z \rangle$ for the spin 3/2 system for (a) $\alpha = 0.5$ and (b) $\alpha = 2$. Similarly to the spin 1 system, noisy Rabi oscillations at low measurement strength are contrasted with fast jumps between the eigenstates at $\langle S_z \rangle = \pm\frac{3}{2}$ and $\langle S_z \rangle = \pm\frac{1}{2}$ when the measurement strength is increased.

## 5. Discussion and conclusions

The QZE has been studied in three open spin systems undergoing Rabi oscillations generated by Hamiltonian $H_s \propto S_x$ and coupled to an environment designed to act as a measurement apparatus for the $S_z$ observable. The interaction between the system and the environment is characterised by a measurement strength $\alpha$. The QSD approach allows the construction of single, physical, stochastic quantum trajectories, and can take into account the effects of measurement in a continuous and explicit manner. The evolution of an open quantum system is therefore modelled using a stochastically evolving (reduced) density matrix, $\rho$, preserving unit trace and positivity. The evolution of the quantum system resembles that of a Brownian particle diffusing across a phase space, and the density matrix, at each instant, is interpreted as a physical property of the system. The average over an ensemble of density matrices represented by the stochastic trajectories is captured by the noise-averaged Lindblad equation.

Stochastic quantum trajectories for the spin 1/2 system have been described in terms of the evolution of the Rabi angle. For the spin 1 and spin 3/2 systems, the evolution of the 'expectation values' $\langle S_y \rangle = Tr(\rho S_y)$ and $\langle S_z \rangle = Tr(\rho S_z)$ were studied. It is important to note that, in

spite of the terminology just used, we regard these spin components as physical properties rather than statistics of an ensemble and that they characterise a single stochastic evolution. To demonstrate the QZE, the spin 1 and spin 3/2 trajectories were analysed to calculate the mean return times under the dynamics, and the residence probabilities, for the various eigenstates of $S_z$.

The stochastic trajectories for both the spin 1 and spin 3/2 systems (figures 4 and 8) reveal a competition between the unitary dynamics which attempt to guide the system along a deterministic trajectory in the $\langle S_y \rangle$, $\langle S_z \rangle$ phase space, and the non-unitary measurement dynamics which seek to divert the system stochastically towards the eigenstates of $S_z$, and dwell in their vicinity. For example, measurement can disturb a deterministic trajectory that passes through eigenstates with the largest eigenvalues, allowing occasional visits to the other eigenstates of $S_z$, such as the $|0\rangle$ eigenstate in the case of the spin 1 system and $|\frac{1}{2}\rangle$ and $|-\frac{1}{2}\rangle$ in the case of the spin 3/2 system. For high enough values of $\alpha$, the system traverses a figure-of-eight path in the case of the spin 1 system, and a triple-figure-of-eight path for the spin 3/2 system. We speculate that a similar pattern will be found for higher spin systems, where for very high values of $\alpha$ the system will simply appear to jump stochastically between the eigenstates. As such, the transition pathways available to the quantum system appear to change according to the strength of the measurement imposed upon it.

The stochastic trajectories generated for all three spin systems for a range of values of the measurement strength $\alpha$ have clearly demonstrated the QZE. With increasing $\alpha$, the mean rate of change of the Rabi angle for the spin 1/2 system decreases (figure 2(a)). Since the Rabi angle describes rotation of the coherence/Bloch vector about an axis specified by the Hamiltonian, such a decrease of its mean rate of change demonstrates a slowing down of the unitary dynamics. Suppression of the unitary dynamics was also illustrated by the increased mean return time to eigenstates in the spin 1 and spin 3/2 systems (figures 7(b) and 9(b). Increased measurement strength causes the system to dwell for longer at each eigenstate, a clear manifestation of the QZE. The stationary PDFs of the spin 1/2 system (figure 3) show that an increase in $\alpha$ narrows the PDFs around the eigenstates of $S_z$.

Probabilities of residence near the eigenstates of $S_z$ for both spin 1 and spin 3/2 systems rise to a ceiling with increasing measurement coupling constant (figures 7(a) and 9(a). At low values of $\alpha$, the system spends significant time exploring phase space away from the eigenstates of $S_z$, but this behaviour becomes rarer as $\alpha$ increases: for example, the spin 3/2 residence probabilities for the four eigenstates rise to about 0.25 for $\alpha > 6$. Such a localisation is also demonstrated by the pattern of stationary probability densities over $\langle S_z \rangle$ and $\langle S_y \rangle$ for spin 1 (figure 5) such that, for high values of $\alpha$, the density is almost exclusively confined to regions of phase space in the vicinity of the three eigenstates. The non-unitary measurement dynamics appear to dominate, localising the system near the eigenstates and supporting the conventional picture of wavefunction collapse.

Notably, in the spin 1 and spin 3/2 systems, the QZE does not manifest itself in the same way for each of the eigenstates of the corresponding $S_z$ observable. Figures 7(b) and 9(b) demonstrate that there is an asymmetry in the dwell and return behaviour for each of the eigenstates of the measured observable. For the eigenstates at the extremities (such as the $|\pm 1\rangle$ eigenstates of the spin 1 system or the $|\pm \frac{3}{2}\rangle$ eigenstates of the spin 3/2 system), the mean return time is roughly double that of the middle eigenstates (for example, the $|0\rangle$ eigenstate of the spin 1 system or the $|\pm \frac{1}{2}\rangle$ eigenstates of the spin 3/2 system) when $\alpha = 7$, thus the QZE manifests itself more strongly for the eigenstates at the extremities. In Bauer *et al*, the jump rates in a strong measurement regime can be calculated, with the inverse yielding an average time between two jumps [34]. Utilising their analytical result for the jump rates, we have found that

the average time between two jumps out of the spin 1 $|\pm 1\rangle$ eigenstates or the $|\pm\frac{3}{2}\rangle$ eigenstates of the spin 3/2 system was roughly double that of the spin 1 $|0\rangle$ eigenstate or the spin 3/2 $|\pm\frac{1}{2}\rangle$ eigenstates, confirming our results for high measurement strength in figures 7(b) and 9(b). Moreover, the measurement strength changes the eigenstates available to the spin 1 and spin 3/2 systems such that in figures 4 and 8, for a low measurement strength only the $|\pm 1\rangle$ or $|\pm\frac{3}{2}\rangle$ respectively are frequently visited. Both of these features could be of use in quantum state control protocols.

Aside from demonstrating the QZE in an open quantum spin system, the QSD framework for generating stochastic quantum trajectories could be used to shed light onto other features of quantum systems such as entanglement, decoherence and measurement back-action. It could also reveal behaviour in more complex systems such as those possessing a memory of past environment-system interactions. Whilst the dynamics of some quantum systems might be well approximated by Markovian stochastic trajectories, future work could consider non-Markovian unravellings or non-Markovian master equations generating stochastic trajectories that are not constrained by the Born-Markov approximation, enabling the study of complex environments with non-negligible correlation times.

## Data availability statement

All data that support the findings of this study are included within the article (and any supplementary files).

## Acknowledgments

S M W is supported by a PhD studentship funded by EPSRC under Grant codes EP/R513143/1 and EP/T517793/1.

## Appendix A. Gell–Mann matrices

The Gell–Mann matrices used to form the spin 1 density matrix in equation (25) are:

$$\lambda_1 = \begin{pmatrix} 0 & 1 & 0 \\ 1 & 0 & 0 \\ 0 & 0 & 0 \end{pmatrix} \lambda_2 = \begin{pmatrix} 0 & -i & 0 \\ i & 0 & 0 \\ 0 & 0 & 0 \end{pmatrix} \lambda_3 = \begin{pmatrix} 1 & 0 & 0 \\ 0 & -1 & 0 \\ 0 & 0 & 0 \end{pmatrix}$$
$$\lambda_4 = \begin{pmatrix} 0 & 0 & 1 \\ 0 & 0 & 0 \\ 1 & 0 & 0 \end{pmatrix} \lambda_5 = \begin{pmatrix} 0 & 0 & -i \\ 0 & 0 & 0 \\ i & 0 & 0 \end{pmatrix} \lambda_6 = \begin{pmatrix} 0 & 0 & 0 \\ 0 & 0 & 1 \\ 0 & 1 & 0 \end{pmatrix}$$
$$\lambda_7 = \begin{pmatrix} 0 & 0 & 0 \\ 0 & 0 & -i \\ 0 & i & 0 \end{pmatrix} \lambda_8 = \frac{1}{\sqrt{3}} \begin{pmatrix} 1 & 0 & 0 \\ 0 & 1 & 0 \\ 0 & 0 & -2 \end{pmatrix}. \tag{A1}$$

## Appendix B. Spin 1 SDEs

Itô processes for the variables parametrising the spin 1 density matrix are as follows:

$$
\begin{aligned}
\mathrm{d}s &= \epsilon\frac{k}{\sqrt{2}}\mathrm{d}t - \alpha^2\frac{s}{2}\mathrm{d}t - \alpha\frac{s}{3}\left(-3+2\sqrt{3}u+6z\right)\mathrm{dW}\\
\mathrm{d}m &= -\epsilon\frac{2u+v}{\sqrt{2}}\mathrm{d}t - \alpha^2\frac{m}{2}\mathrm{d}t - \alpha\frac{m}{3}\left(-3+2\sqrt{3}u+6z\right)\mathrm{dW}\\
\mathrm{d}u &= \epsilon\frac{2m-y}{\sqrt{2}}\mathrm{d}t + \alpha\frac{1}{\sqrt{3}}\left(1-2u^2+\sqrt{3}u(1-2z)+z\right)\mathrm{dW}\\
\mathrm{d}v &= \epsilon\frac{m-y}{\sqrt{2}}\mathrm{d}t - 2\alpha^2 v\mathrm{d}t - \frac{2}{3}\alpha v\left(\sqrt{3}u+3z\right)\mathrm{dW}\\
\mathrm{d}k &= \epsilon\frac{-s+x}{\sqrt{2}}\mathrm{d}t - 2\alpha^2 k\mathrm{d}t - \frac{2}{3}\alpha k\left(\sqrt{3}u+3z\right)\mathrm{dW}\\
\mathrm{d}x &= -\epsilon\frac{k}{\sqrt{2}}\mathrm{d}t - \frac{1}{2}\alpha^2 x\mathrm{d}t - \frac{1}{3}\alpha x\left(3+2\sqrt{3}u+6z\right)\mathrm{dW}\\
\mathrm{d}y &= \epsilon\frac{u+v-\sqrt{3}z}{\sqrt{2}}\mathrm{d}t - \frac{1}{2}\alpha^2 y\mathrm{d}t - \frac{1}{3}\alpha y\left(3+2\sqrt{3}u+6z\right)\mathrm{dW}\\
\mathrm{d}z &= \epsilon\sqrt{\frac{3}{2}}y\mathrm{d}t - \frac{1}{3}\alpha(-1+2z)\left(3+\sqrt{3}u+3z\right)\mathrm{dW}.
\end{aligned}
\tag{B1}
$$

## Appendix C. Spin 3/2 generators

The SU(2)⊗SU(2) generators used to form the spin 3/2 density matrix in equation (28) are as follows: $\Sigma_1 = I_2\otimes\sigma_x$, $\Sigma_2 = I_2\otimes\sigma_y$, $\Sigma_3 = I_2\otimes\sigma_z$, $\Sigma_4 = \sigma_x\otimes I_2$, $\Sigma_5 = \sigma_x\otimes\sigma_x$, $\Sigma_6 = \sigma_x\otimes\sigma_y$, $\Sigma_7 = \sigma_x\otimes\sigma_z$, $\Sigma_8 = \sigma_y\otimes I_2$, $\Sigma_9 = \sigma_y\otimes\sigma_x$, $\Sigma_{10} = \sigma_y\otimes\sigma_y$, $\Sigma_{11} = \sigma_y\otimes\sigma_z$, $\Sigma_{12} = \sigma_z\otimes I_2$, $\Sigma_{13} = \sigma_z\otimes\sigma_x$, $\Sigma_{14} = \sigma_z\otimes\sigma_y$ and $\Sigma_{15} = \sigma_z\otimes\sigma_z$, where $I_2$ is a $2\times 2$ identity matrix. Explicitly:

$$
\Sigma_1 = \begin{pmatrix} 0&1&0&0\\ 1&0&0&0\\ 0&0&0&1\\ 0&0&1&0\end{pmatrix}\quad
\Sigma_2 = \begin{pmatrix} 0&-i&0&0\\ i&0&0&0\\ 0&0&0&-i\\ 0&0&i&0\end{pmatrix}
$$

$$
\Sigma_3 = \begin{pmatrix} 1&0&0&0\\ 0&-1&0&0\\ 0&0&1&0\\ 0&0&0&-1\end{pmatrix}\quad
\Sigma_4 = \begin{pmatrix} 0&0&1&0\\ 0&0&0&1\\ 1&0&0&0\\ 0&1&0&0\end{pmatrix}
$$

$$
\Sigma_5 = \begin{pmatrix} 0&0&0&1\\ 0&0&1&0\\ 0&1&0&0\\ 1&0&0&0\end{pmatrix}\quad
\Sigma_6 = \begin{pmatrix} 0&0&0&-i\\ 0&0&i&0\\ 0&-i&0&0\\ i&0&0&0\end{pmatrix}
$$

$$
\Sigma_7 = \begin{pmatrix} 0&0&1&0\\ 0&0&0&-1\\ 1&0&0&0\\ 0&-1&0&0\end{pmatrix}\quad
\Sigma_8 = \begin{pmatrix} 0&0&-i&0\\ 0&0&0&-i\\ i&0&0&0\\ 0&i&0&0\end{pmatrix}
$$

$$\Sigma_9 = \begin{pmatrix} 0 & 0 & 0 & -i \\ 0 & 0 & -i & 0 \\ 0 & i & 0 & 0 \\ i & 0 & 0 & 0 \end{pmatrix} \Sigma_{10} = \begin{pmatrix} 0 & 0 & 0 & -1 \\ 0 & 0 & 1 & 0 \\ 0 & -1 & 0 & 0 \\ 1 & 0 & 0 & 0 \end{pmatrix}$$
$$\Sigma_{11} = \begin{pmatrix} 0 & 0 & -i & 0 \\ 0 & 0 & 0 & i \\ i & 0 & 0 & 0 \\ 0 & -i & 0 & 0 \end{pmatrix} \Sigma_{12} = \begin{pmatrix} 1 & 0 & 0 & 0 \\ 0 & 1 & 0 & 0 \\ 0 & 0 & -1 & 0 \\ 0 & 0 & 0 & -1 \end{pmatrix}$$
$$\Sigma_{13} = \begin{pmatrix} 0 & 1 & 0 & 0 \\ 1 & 0 & 0 & 0 \\ 0 & 0 & 0 & -1 \\ 0 & 0 & -1 & 0 \end{pmatrix} \Sigma_{14} = \begin{pmatrix} 0 & -i & 0 & 0 \\ i & 0 & 0 & 0 \\ 0 & 0 & 0 & i \\ 0 & 0 & -i & 0 \end{pmatrix}$$
$$\Sigma_{15} = \begin{pmatrix} 1 & 0 & 0 & 0 \\ 0 & -1 & 0 & 0 \\ 0 & 0 & -1 & 0 \\ 0 & 0 & 0 & 1 \end{pmatrix}. \tag{C1}$$

## Appendix D. Spin 3/2 SDEs

Itô processes for the variables parametrising the spin 3/2 density matrix are as follows:

$$\begin{aligned}
\mathrm{d}v &= -\epsilon o\mathrm{d}t - \frac{1}{2}\alpha^2 v\mathrm{d}t + \alpha(2q - v(f+2p)\mathrm{dW} \\
\mathrm{d}e &= \epsilon(\sqrt{3}f + k)\mathrm{d}t - \frac{1}{2}\alpha^2 e\mathrm{d}t + \alpha(2s - e(f+2p))\mathrm{dW} \\
\mathrm{d}f &= -\epsilon(\sqrt{3}e + j - m)\mathrm{d}t - \alpha(-1 + f^2 + 2fp - 2u)\mathrm{dW} \\
\mathrm{d}g &= -\epsilon s\mathrm{d}t - 2\alpha^2 g\mathrm{d}t + \alpha(k - g(f+2p))\mathrm{dW} \\
\mathrm{d}h &= -\frac{1}{2}\alpha^2(5h - 4n)\mathrm{d}t - \alpha h(f+2p)\mathrm{dW} \\
\mathrm{d}j &= \epsilon(f + \sqrt{3}k - p)\mathrm{d}t - \frac{1}{2}\alpha^2(5j + 4m)\mathrm{d}t - \alpha j(f+2p)\mathrm{dW} \\
\mathrm{d}k &= -\epsilon(e + \sqrt{3}j)\mathrm{d}t - 2\alpha^2 k\mathrm{d}t + \alpha(g - k(f+2p))\mathrm{dW} \\
\mathrm{d}l &= \epsilon q\mathrm{d}t - 2\alpha^2 l\mathrm{d}t + \alpha(o - l(f+2p))\mathrm{dW} \\
\mathrm{d}m &= \epsilon(-f + p)\mathrm{d}t - \frac{1}{2}\alpha^2(4j + 5m)\mathrm{d}t - \alpha m(f+2p)\mathrm{dW} \\
\mathrm{d}n &= \epsilon\sqrt{3}o\mathrm{d}t + \alpha^2\left(2h - \frac{5n}{2}\right)\mathrm{d}t - \alpha n(f+2p)\mathrm{dW} \\
\mathrm{d}o &= \epsilon(-\sqrt{3}n + v)\mathrm{d}t - 2\alpha^2 o\mathrm{d}t + \alpha(l - o(f+2p))\mathrm{dW} \\
\mathrm{d}p &= \epsilon(j - m)\mathrm{d}t + \alpha(2 - p(f+2p) + u)\mathrm{dW} \\
\mathrm{d}q &= -\epsilon l\mathrm{d}t - \frac{1}{2}\alpha^2 q\mathrm{d}t - \alpha(fq + 2pq - 2v)\mathrm{dW} \\
\mathrm{d}s &= \epsilon(g + \sqrt{3}u)\mathrm{d}t - \frac{1}{2}\alpha^2 s\mathrm{d}t + \alpha(2e - s(f+2p))\mathrm{dW} \\
\mathrm{d}u &= -\epsilon\sqrt{3}s\mathrm{d}t + \alpha(2f + p - u(f+2p))\mathrm{dW}.
\end{aligned} \tag{D1}$$

## ORCID iD

Sophia M Walls https://orcid.org/0000-0002-2205-059X

## References

[1] Degasperis A, Fonda L and Ghirardi G C 1974 Does the lifetime of an unstable system depend on the measuring apparatus? *Il Nuovo Cimento* A **21** 471
[2] Misra B and Sudarshan E C G 1977 The Zeno's paradox in quantum theory *J. Math. Phys.* **18** 756
[3] Zhang M, Wu C, Xie Y, Wu W and Chen P 2019 Quantum Zeno effect by incomplete measurements *Quantum Inf. Process.* **18** 97
[4] Peres A and Ron A 1990 Incomplete "collapse" and partial quantum Zeno effect *Phys. Rev.* A **42** 5720
[5] Oliveira M H, Higgins G, Zhang C, Predojević A, Hennrich M, Bachelard R and Villas-Boas C J 2022 Steady-state entanglement generation for non-degenerate qubits (arXiv:2205.10590 [quant-ph])
[6] Salih H, Hance J R, McCutcheon W, Rudolph T and Rarity J 2021 Deterministic teleportation and universal computation without particle exchange (arXiv:2009.05564 [quant-ph])
[7] Chen Y-H and Brun T A 2020 Continuous quantum error detection and suppression with pairwise local interactions *Phys. Rev. Res.* **2** 043093
[8] Li Y, Chen X and Fisher M P A 2018 Quantum Zeno effect and the many-body entanglement transition *Phys. Rev.* B **98** 205136
[9] Lin J-D, Huang C-Y, Lambert N, Chen G-Y, Nori F and Chen Y-N 2022 Space-time dual quantum Zeno effect: interferometric engineering of open quantum system dynamics (arXiv:2208.02472 [quant-ph])
[10] Long X *et al* 2022 Entanglement-enhanced quantum metrology in colored noise by quantum Zeno effect *Phys. Rev. Lett.* **129** 070502
[11] Blumenthal E, Mor C, Diringer A A, Martin L S, Lewalle P, Burgarth D, Whaley K B and Hacohen-Gourgy S 2021 Demonstration of universal control between non-interacting qubits using the quantum Zeno effect (arXiv:2108.08549 [quant-ph])
[12] Nodurft I C, Shaw H C, Glasser R T, Kirby B T and Searles T A 2022 Generation of polarization entanglement via the quantum Zeno effect (arXiv:2205.02315 [quant-ph])
[13] Leppenen N V and Smirnov D S 2022 Optical measurement of electron spins in quantum dots: quantum Zeno effects (arXiv:2202.13994 [cond-mat, physics:quant-ph])
[14] Patsch S, Maniscalco S and Koch C P 2020 Simulation of open-quantum-system dynamics using the quantum Zeno effect *Phys. Rev. Res.* **2** 023133
[15] Bethke P, McNeil R P G, Ritzmann J, Botzem T, Ludwig A, Wieck A D and Bluhm H 2020 Measurement of backaction from electron spins in a gate-defined GaAs double quantum dot coupled to a mesoscopic nuclear spin bath *Phys. Rev. Lett.* **125** 047701
[16] Madzik M T *et al* 2020 Controllable freezing of the nuclear spin bath in a single-atom spin qubit *Sci. Adv.* **6** eaba3442
[17] Norsen T 2017 *Foundations of Quantum Mechanics: An Exploration of the Physical Meaning of Quantum Theory* (Springer)
[18] Jacobs K 2014 *Quantum Measurement Theory and Its Applications* (Cambridge University Press)
[19] Murch K W, Weber S J, Macklin C and Siddiqi I 2013 Observing single quantum trajectories of a superconducting quantum bit *Nature* **502** 211
[20] Jordan A N 2013 Watching the wavefunction collapse *Nature* **502** 177
[21] Bellini M, Kwon H, Biagi N, Francesconi S, Zavatta A and Kim M S 2022 Demonstrating quantum microscopic reversibility using coherent states of light (arXiv:2205.13089 [quant-ph])
[22] Gross J A, Baragiola B Q, Stace T M and Combes J 2022 Master equations and quantum trajectories for squeezed wave packets *Phys. Rev.* A **105** 023721
[23] Minev Z K, Mundhada S O, Shankar S, Reinhold P, Gutiérrez-Jáuregui R, Schoelkopf R J, Mirrahimi M, Carmichael H J and Devoret M H 2019 To catch and reverse a quantum jump mid-flight *Nature* **570** 200
[24] Presilla C, Onofrio R and Tambini U 1996 Measurement quantum mechanics and experiments on quantum Zeno effect *Ann. Phys., NY* **248** 95

[25] Itano W M, Heinzen D J, Bollinger J J and Wineland D J 1990 Quantum Zeno effect *Phys. Rev.* A **41** 2295
[26] Snizhko K, Kumar P and Romito A 2020 Quantum Zeno effect appears in stages *Phys. Rev. Res.* **2** 033512
[27] Gambetta J, Blais A, Boissonneault M, Houck A A, Schuster D I and Girvin S M 2008 Quantum trajectory approach to circuit QED: quantum jumps and the Zeno effect *Phys. Rev.* A **77** 012112
[28] de Vega I and Alonso D 2017 Dynamics of non-Markovian open quantum systems *Rev. Mod. Phys.* **89** 015001
[29] Christie R, Eastman J, Schubert R and Graefe E-M 2022 Quantum-jump vs stochastic Schrödinger dynamics for Gaussian states with quadratic Hamiltonians and linear Lindbladians *J. Phys. A: Math. Theor.* **55** 455302
[30] Gardiner C W, Parkins A S and Zoller P 1992 Wave-function quantum stochastic differential equations and quantum-jump simulation methods *Phys. Rev.* A **46** 4363
[31] Gneiting C, Rozhkov A V and Nori F 2021 Jump-time unraveling of Markovian open quantum systems *Phys. Rev.* A **104** 062212
[32] Percival I 1998 *Quantum State Diffusion* (Cambridge University Press)
[33] Gisin N and Percival I C 1992 The quantum-state diffusion model applied to open systems *J. Phys. A: Math. Gen.* **25** 5677
[34] Bauer M, Bernard D and Tilloy A 2015 Computing the rates of measurement-induced quantum jumps *J. Phys. A: Math. Theor.* **48** 25FT02
[35] Spiller T P 1994 The Zeno effect: measurement versus decoherence *Phys. Lett.* A **192** 163
[36] Penrose R 2014 On the gravitization of quantum mechanics 1: quantum state reduction *Found. Phys.* **44** 557
[37] Ghirardi G C, Rimini A and Weber T 1986 Unified dynamics for microscopic and macroscopic systems *Phys. Rev.* D **34** 470
[38] Bohm D 1952 A suggested interpretation of the quantum theory in terms of 'hidden' variables. I *Phys. Rev.* **85** 166
[39] Saunders S, Barrett J, Kent A and Wallace D 2010 *Many Worlds?: Everett, Quantum Theory, & Reality* (OUP Oxford)
[40] Everett H 1957 'Relative state' formulation of quantum mechanics *Rev. Mod. Phys.* **29** 454
[41] Bassi A, Lochan K, Satin S, Singh T P and Ulbricht H 2013 Models of wave-function collapse, underlying theories and experimental tests *Rev. Mod. Phys.* **85** 471
[42] Pusey M F, Barrett J and Rudolph T 2012 On the reality of the quantum state *Nat. Phys.* **8** 475
[43] Lombardi O and Dieks D 2021 Modal interpretations of quantum mechanics *The Stanford Encyclopedia of Philosophy* winter edn ed E N Zalta (Metaphysics Research Lab, Stanford University)
[44] Petersen A 1963 The Philosophy of Niels Bohr *Bull. At. Sci.* **19** 8
[45] Fuchs C A, Mermin N D and Schack R 2014 An introduction to QBism with an application to the locality of quantum mechanics *Am. J. Phys.* **82** 749
[46] Pitowsky I 2005 Quantum mechanics as a theory of probability (arXiv:quant-ph/0510095)
[47] Healey R 2012 Quantum theory: a pragmatist approach *Br. J. Phil. Sci.* **63** 729
[48] Harrigan N and Spekkens R W 2010 Einstein, incompleteness and the epistemic view of quantum states *Found. Phys.* **40** 125
[49] Kochen S and Specker E P 1967 The problem of hidden variables in quantum mechanics *J. Math. Mech.* **17** 59–87
[50] Brukner C and Zeilinger A 2002 Information and fundamental elements of the structure of quantum theory (arXiv:quant-ph/0212084)
[51] Mermin N D 2013 Annotated interview with a QBist in the making (arXiv:1301.6551 [physics, physics:quant-ph])
[52] Rovelli C 2021 *Helgoland* (Penguin Books)
[53] Maudlin T 2019 *Philosophy of Physics: Quantum Theory* (*Princeton Foundations of Contemporary Philosophy*) (Princeton University Press)
[54] Leifer M S 2014 Is the quantum state real? an extended review of $\psi$-ontology theorems *Quanta* **3** 67
[55] Hiley B J, Callaghan R E and Maroney O 2000 Quantum trajectories, real, surreal or an approximation to a deeper process? (arXiv:quant-ph/0010020)
[56] Wiseman H M 1996 Quantum trajectories and quantum measurement theory *Quantum Semiclass. Opt. J. Eur. Opt. Soc.* B **8** 205

[57] Gambetta J and Wiseman H M 2003 Interpretation of non-Markovian stochastic Schrödinger equations as a hidden-variable theory *Phys. Rev.* A **68** 062104
[58] Breuer H-P and Petruccione F 2007 *The Theory of Open Quantum Systems* (Oxford University Press)
[59] Matos D, Kantorovich L and Ford I J 2022 Stochastic entropy production for continuous measurements of an open quantum system *J. Phys. Commun.* **6** 125003
[60] Clarke C L 2022 *Irreversibility Measures in a Quantum Setting Doctoral, UCL* University College London
[61] Gross J A, Caves C M, Milburn G J and Combes J 2018 Qubit models of weak continuous measurements: Markovian conditional and open-system dynamics *Quantum Sci. Technol.* **3** 024005
[62] Helmer F, Mariantoni M, Solano E and Marquardt F 2009 Quantum nondemolition photon detection in circuit QED and the quantum Zeno effect *Phys. Rev.* A **79** 052115
[63] Itô K 1944 Stochastic integral *Proc. Imperial Acad.* **20** 519
[64] Aerts D and Sassoli de Bianchi M 2014 The extended Bloch representation of quantum mechanics and the hidden-measurement solution to the measurement problem *Ann. Phys., NY* **351** 975
[65] Lukach I and Smorodinskij Ya A 1978 On algebra of Gell-Mann's matrices for SU(3) group *Sov. J. Nucl. Phys.* **27** 1694–702
[66] Kloeden P E and Platen E 1992 Stochastic differential equations *Numerical Solution of Stochastic Differential Equations* (*Applications of Mathematics*) ed P E Kloeden and E Platen (Springer)
[67] (Available at: https://drive.google.com/file/d/1xcBIlHtQ-pseZNxMxSvL-PG60BxXxLNH/view?usp=sharingMovieofspin1dynamicswithmeasurementstrength3)
[68] (Available at: https://drive.google.com/file/d/1sNncxc19eDs8ZXe5Pt66LE_fIHOMlT_v/view?usp=sharingMovieofspin3/2dynamicswithmeasurementstrength1)